Navigating the Carbon Maze: A Roadmap to Effective Carbon Conductive Networks for Lithium-Ion Batteries

Review Article

Author(s):
Baumgärtner, Julian F.; Kravchyk, Kostiantyn V.; Kovalenko, Maksym V.

Publication date:
2024

Permanent link:
https://doi.org/10.3929/ethz-b-000670529

Originally published in:
Advanced Energy Materials, https://doi.org/10.1002/aenm.202400499

ADVANCED ENERGY MATERIALS
www.advenergymat.de

Navigating the Carbon Maze: A Roadmap to Effective Carbon Conductive Networks for Lithium-Ion Batteries

*Julian F. Baumgärtner, Kostiantyn V. Kravchyk, and Maksym V. Kovalenko**

Conductive networks are integral components in Li-ion battery electrodes, serving the dual function of providing electrons to the active material while its porosity ensures Li-ion electrolyte accessibility to deliver and release Li-ions, thereby ultimately determining the electrochemical performance of the battery. In the realm of academic research, the task of fabricating an electrode endowed with an effective conductive network has emerged as a daunting challenge, profoundly influencing a researcher's ability to showcase the intrinsic electrochemical performance of an active material. In the diverse landscape of conductive additives for battery electrodes, researchers are faced with a myriad of options when deciding on the appropriate additive and optimal electrode preparation methodology. This review seeks to provide a fundamental understanding and practical guidelines for designing battery electrodes with effective conductive networks across various length scales. This involves the meticulous selection of specific carbon conductive additives from the plethora of options and the exploration of methods for their effective integration into the electrode, all tailored to the unique characteristics of the active materials and the specific research objectives.

1. Introduction

Li-ion batteries (LIBs) are an integral part of modern energy-storage solutions, powering a spectrum of devices from consumer electronics and power tools to electric vehicles (EVs). Despite consistent advancements in LIBs performance, the challenges posed by demanding applications in mobility persist.[1] EVs, in particular, necessitate high-energy densities (>500 Wh L^{-1} and >230 Wh kg^{-1}), fast charging times (10 to 15 min), and stability over hundreds of charging cycles to match the mileage, recharge times, and durability of internal combustion engine vehicles.[2,3] Improving the energy and power density, along with the cycling stability of current LIBs, through the development of novel active materials or enhanced utilization of current active materials, stands as a critical challenge.

At the heart of these challenges lies the intricate interplay of electron and ion transport.[4,5] While active material selection theoretically determines the thermodynamic open circuit voltage and energy density of the prospective battery, transport processes kinetically limit the achievable voltage and charge storage capacity at a given C rate. A well-designed conductive network should therefore aim to minimize kinetic limitations by efficiently providing electrons to the active material while its porosity ensures accessibility for the liquid electrolyte to deliver and release Li-ions to the active material.

In the field of academic research, producing electrodes with an efficient conductive network is a complex task, significantly affecting a researcher's capacity to demonstrate the inherent electrochemical capabilities of emerging active materials. Amidst the plethora of conductive additives available for battery electrodes, researchers often find themselves navigating a maze of choices when trying to determine the appropriate additive and the optimal electrode fabrication method. Yet, experimental descriptions in research papers detailing the electrode fabrication based on novel active materials frequently offer surprisingly limited information, such as: "Electrodes were fabricated by ball milling active material (xx wt.-%), conductive additive (yy wt.-%) and pVdF binder (zz wt.-%) in NMP."[6–12] Newcomers to the field may therefore wrongfully conclude that the choice of conductive additive and electrode fabrication method are insignificant as long as all components are well dispersed, the carbon content is sufficiently high, and the loading of active materials is kept low.

This review addresses this issue by summarizing the theoretical framework and establishing simple and intuitive guidelines for the preparation of battery electrodes with effective conductive networks, employing various carbon conductive

J. F. Baumgärtner, K. V. Kravchyk, M. V. Kovalenko
Laboratory of Inorganic Chemistry
Department of Chemistry and Applied Biosciences
ETH Zürich
Vladimir-Prelog-Weg 1, Zürich CH-8093, Switzerland
E-mail: mvkovalenko@ethz.ch
J. F. Baumgärtner, K. V. Kravchyk, M. V. Kovalenko
Laboratory for Thin Films and Photovoltaics
Empa – Swiss Federal Laboratories for Materials Science and Technology
Überlandstrasse 129, Dübendorf CH-8600, Switzerland
M. V. Kovalenko
Institute of Energy Science and Technology (SIEST)
Sungkyunkwan University (SKKU)
2066, Seobu-ro, Jangan-gu, Suwon, Gyeonggi-do 16419, Republic of Korea

The ORCID identification number(s) for the author(s) of this article can be found under https://doi.org/10.1002/aenm.202400499

DOI: 10.1002/aenm.202400499

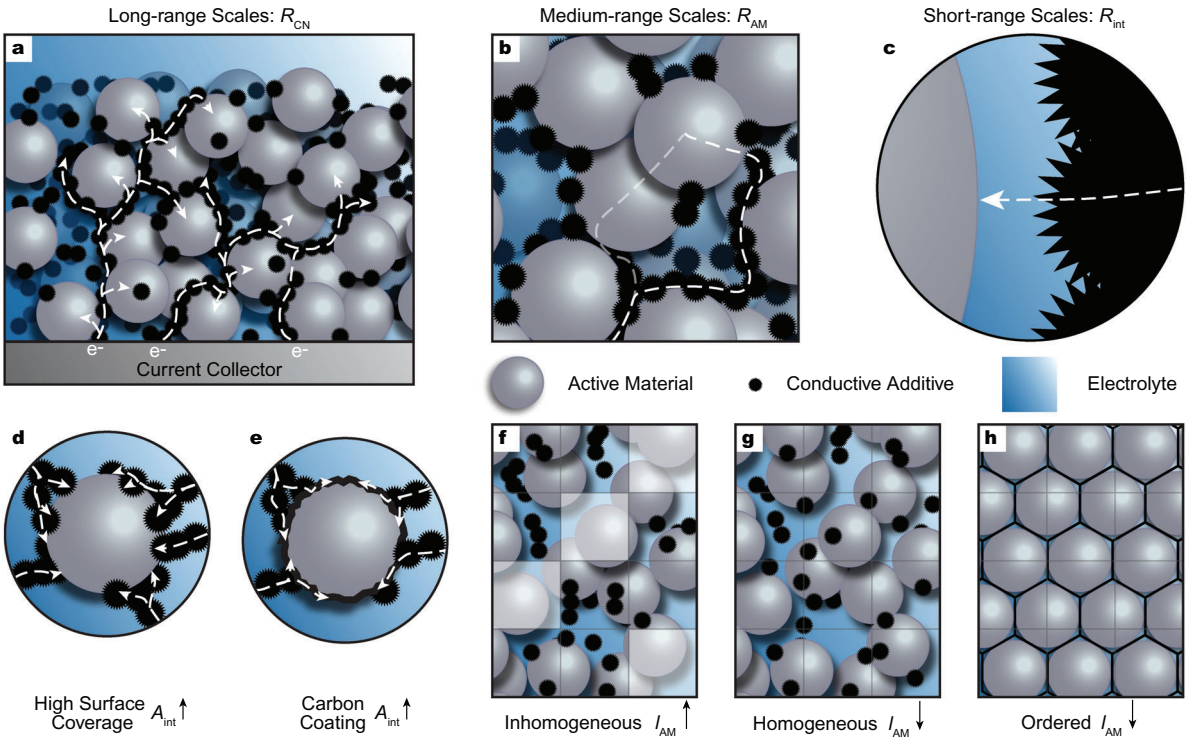

Figure 1. Electronic conduction inside the conductive network across different length scales. a–c) Electronic conduction on the long-range scale through the conductive network (a), on the medium-range scale through the active material (b), and on the short-range scale across the interface c). d,e) Increasing the interfacial contact area between active material and conductive network by high surface coverage (d) and carbon coating (e). f–h) Influencing the diffusion length through the active material by inhomogeneous conductive network distribution (f), homogeneous conductive network distribution (g), and ordered conductive networks (h).

additives. The review is designed to be applicable for electrode fabrication with both state-of-the-art and emerging active materials. While there are excellent reviews describing the physicochemical properties of individual components of a conductive network such as carbon black (CB),[13–15] carbon nanotubes (CNTs),[16–18] or graphene,[16,19,20] to our knowledge, no review has yet delved into the theoretical and practical design of effective carbon conductive networks derived from multiple conductive additives.

This review begins with an overview of the physics of electronic transport across different length scales in Section 2. We outline the relevant theories and their implications for constructing effective conductive networks. Section 3 provides an overview of various conductive additives and carbon coatings as the basic building blocks of conductive networks, covering their physicochemical properties and how they relate to electrochemical performance. Section 4 reviews the structure and preparation of electrodes using commercial active materials, scrutinizing the structure and stability of state-of-the-art electrodes and exploring emerging strategies in the field. We also highlight the importance of defining the scope of what "effective" means in any particular application, depending on the optimization for high-energy and high-power density, and across different technology readiness levels (TRLs). Section 5 extends the discussion to novel active materials, outlining challenges and proposing strategies for developing conductive networks. Ultimately, guidelines for the construction of electrodes are presented in Section 6. The review concludes with the key takeaways, alongside cautionary considerations when preparing electrodes and interpreting electrochemical results.

2. Electronic Conduction in Conductive Networks

To maximize the rate capability of a cell, the electronically conductive network must ensure efficient electronic conduction within the electrode, facilitating the delivery and release of electrons to the surface of the active material, thereby minimizing the overall cell resistance (**Figure 1**a–c). Concomitantly, a conductive network must be porous, fostering effective ionic transport to the active material without inadvertently impeding access to the electrolyte.[13,21] Several insightful reviews underscore the significance of porous conductive networks in optimizing Li-ion transport within battery electrodes.[4,5,22–25] Nevertheless, the aspect of electronic conduction within these networks has been less explored, despite its equal importance in identifying and mitigating bottlenecks for high rate capability. Consequently, the subsequent discussion delves into the fundamental theory of electronic conduction in porous conductive networks.

The total electronic cell resistance R_{tot} is the sum of three components: i) the resistance of the conductive network R_{CN}, ii) the resistance within the active material R_{AM}, and iii) the resistance across an interface between the conductive network and the active material R_{int}, according to Equation 1:[26–28]

$$R_{tot} = R_{CN} + R_{AM} + R_{int} \quad \text{where} \quad R_i = \frac{l_i}{\sigma_i \cdot A_i} \tag{1}$$

where l_i, A_i and σ_i are the effective length, cross sectional area, and electronic conductivity of each component, respectively. Equation 1 assumes an electron that travels in sequence along a path of all three components (Figure 1a–c). This model does not explicitly treat the many parallel circuits required to model a real electrode, and it neglects the capacitive contribution to the overall impedance. To account for these effects, transmission line models can be used to study the effect of individual components on the overall impedance,[29–32] and interested readers are referred to a recent review by Gaberšček et al.[33] However, this simplified model is more valuable to gain an intuitive understanding of electronic transport in electrodes, with the aim to formulate guidelines for the construction of effective conductive networks from it.

Electronic conductivity in the conductive network (σ_{CN}) is orders of magnitude higher than in most active materials. For instance, the room-temperature conductivity of common active materials (σ_{AM}) are 0.5 S cm^{-1} for Lithium Cobalt Oxide (LCO),[34] 10^{-2} S cm^{-1} for Lithium nickel cobalt oxide (NCO),[35] 10^{-3} S cm^{-1} for Lithium nickel manganese cobalt oxide (NMC),[36] 10^{-5} S cm^{-1} for Lithium iron phosphate (LFP),[37] 10^{-4} S cm^{-1} for Lithium manganese oxide (LMO),[38] 10^{-29} S cm^{-1} for sulfur, or 10^{-3} S cm^{-1} for silicon. By comparison, conductive additives have conductivities of 10^2 to 10^5 S cm^{-1}.[39] Electrons therefore travel the vast majority of the total distance (µm to mm) in the conductive network (l_{CN}) and minimize electronic diffusion pathways in the active materials (l_{AM}) to a few nm to µm (Figure 1a,b). We denote those distinct length scales as long- and medium-range length scales. Close proximity of every active material particle to the conductive network is therefore required on a medium-range scale.[13,21,40,41] Lastly, conduction across interfaces occurs on the atomic level (Å to nm), i.e., on the short-range scale (Figure 1c). Design considerations for the conductive network on these three length scales are considered in depth in the following sections, moving from short- to medium and, finally, long-range scales.

2.1. Short-Range Lengths Scales in Conductive Networks

A conductive network might have an excellent percolating network, with all of the active material nanosized and in close spatial contact with the conductive network, but if the interfacial resistance between the active material and conductive network is high, the cell capacity will only be a fraction of the theoretical capacity. The cross sectional area (A_{int}) is dictated by the distance between the conductive network and active material, over which electron tunneling is feasible, usually only a few Å (Figure 1c). Conductive networks and active material particles have irregular microstructures, so simple point contacts between the two result in small cross sectional areas and therefore large interfacial resistances (R_{int}).

Large cross sectional areas are therefore required to improve interfacial contact, for instance through high carbon coverage of the active material surface. Alternatively, carbon coatings can provide very large contact areas with the active material and therefore effective electronic contact (Figure 1d,e). It is noteworthy that interfacial resistances may still be high if interfacial conductivities (σ_{int}) are low due to the presence of resistive cathode electrolyte, or solid electrolyte interphases. However, these are related to the active material and therefore out of the scope of this review.

2.2. Medium-Range Lengths Scales in Conductive Networks

To illustrate the importance of conductivity on medium-range scales, imagine two possible pathways by which an electron can be delivered to the active material (Figure 1b). In this thought experiment, interfacial resistances between active material and conductive network are briefly neglected but have been considered in the previous section. Along the optimal path, this sum of resistances is minimized according to Equation 1. Because the conductive network and the active material have conductivities that are orders of magnitude different from each other, the electron travels the vast majority of its distance within the conductive network and minimizes the distance traveled in the active material (Figure 1a,b). To facilitate high rate capability, an ideal conductive network should therefore minimize the average distance between any point in the active material to the nearest point in the conductive network.

This notion is captured by the requirement of a homogeneously distributed conductive network. To illustrate this, we subdivide the electrode into subvolume cubes with edge lengths roughly equal to the smallest active material particle dimension (Figure 1f,g). A homogeneously distributed conductive network branches into every subvolume of the electrode to limit the maximum distance an electron travels within the active material to at most the active particle diameter.

Further reduction of the resistance is possible by rigorously minimizing the electron path travelled within the active material under the boundary condition of minimum use of the conductive additive. This optimization is equivalent to an optimal tessellation of space with regular polyhedra. To illustrate this point visually, consider the simplified 2D case of an ordered conductive network with a regular hexagonal closed packing (Figure 1h). In this case, the maximum distance an electron needs to travel within the active material is, at most, the inradius of the hexagon. This thought experiment demonstrates how ordered conductive networks can be considerably more favorable to deliver electrons to the entire active material effectively, especially for very poorly conductive active materials. The ability to do so, as measured by the average distance between any point in the active material to the nearest point in the conductive network, should therefore be another important metric to compare the quality of different conductive networks.

Interestingly, carbon coatings limit the maximum distance that an electron needs to travel within the active material before reaching the conductive network to just the particle radius and therefore fulfill the requirement of optimal conductivity on medium-range scales.

2.3. Long-Range Length Scales in Conductive Networks

To describe the long-range electronic conduction throughout the entire conductive network, one can use the intuitive approach based on the stepwise addition of discrete conductive additive

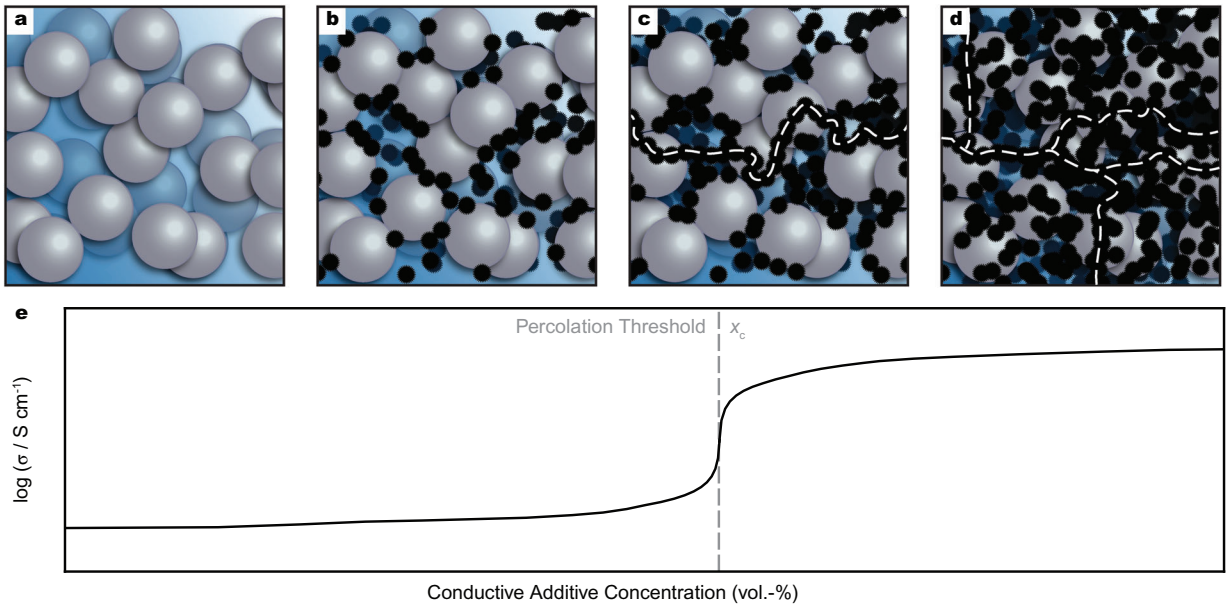

Figure 2. Schematic presentation of a percolation curve at various conductive additive contents. a–d) Schematic presentation of the electrode structure at various carbon contents. e) Theoretical percolation curve of the electronic conduction of the composite at various carbon concentrations. Adapted with permission.[13] Copyright 2022, Elsevier.

particles that are mixed together with other predominantly non-conductive materials to form an electrode. Macroscopic conductivity arises if the conductive building units form a percolating network throughout the entire composite. To illustrate this, consider an electrode without any conductive additive to which the conductive additive is added stepwise in random locations (**Figure 2**a). Initially, the composite is electrically insulating because no conductive additive is present. When conductive additive is now added randomly to the system, the particles are initially not connected, so the composite is still insulating. Upon further addition, the percolation threshold is reached and a connected conductive path throughout the entire composite is formed. At the percolation threshold, the entire composite switches from being insulating to being conductive (Figure 2c,e). Adding more conductive additives beyond the percolation threshold still improves conductivity because the pathways become less tortuous and more numerous, thereby increasing the cross sectional area for conduction.

How electronic percolation arises in a composite of two phases with different conductivity, can be described mathematically by different theories. The most widely used ones are percolation theory (PT),[42–46] and effective medium theory (EMT).[44,47,48] Both theories have important implications for the design of conductive networks and are discussed below.

2.3.1. Percolation Theory

PT theory was first used to describe gelation in polymers,[45] and was later generalized to describe networks that undergo a phase transition once a critical number of nodes, the percolation threshold, is connected within the system.[42,43,49] PT is therefore particularly insightful for the preparation of electrodes because it predicts the minimum required amount of conductive additive to achieve electronic percolation, which is especially relevant for high-power and high-energy density applications. Consequently, PT has found wide application in materials science to describe the formation of conductive networks within composites, e.g. polymer composites,[47,50–53] fuel cells, or battery electrodes.[15,54–59]

The conductivity of the composite σ above the percolation threshold x_c can be expressed by a power law:[60]

$$\sigma \propto \sigma_0 \cdot \left(x - x_c\right)^n \tag{2}$$

where σ_0 is the effective conductivity of the conductive additive, x is the volumetric concentration of the conductive additive and n is the critical exponent with a theoretic value of $n = 2$.

Important insights about conductive networks arise from Equation 2 and are summarized in **Figure 3**a–d. The first and most obvious implication is that adding larger amounts of conductive additive directly increases the conductivity within the electrode. However, the conductivity increase from adding more conductive additive diminishes after the percolation threshold. Therefore, adding significantly more conductive additive beyond the percolation threshold does not improve the macroscopic electrode conductivity meaningfully. Second, a conductive additive with high intrinsic conductivity improves the conductivity in the overall composite. Apart from these two obvious requirements, PT also has more subtle implications about how to lower the percolation threshold x_c.

First, the particle size ratio between active material and conductive additive is inversely proportional to the percolation threshold (Figure 3b). For spherical particles of equal size, a universal percolation threshold of ca. 16 vol.-% is found.[63] However, this value is significantly reduced if the size of the conductive additive particles relative to the active material is reduced. In this case, a large amount of the total volume is excluded, so

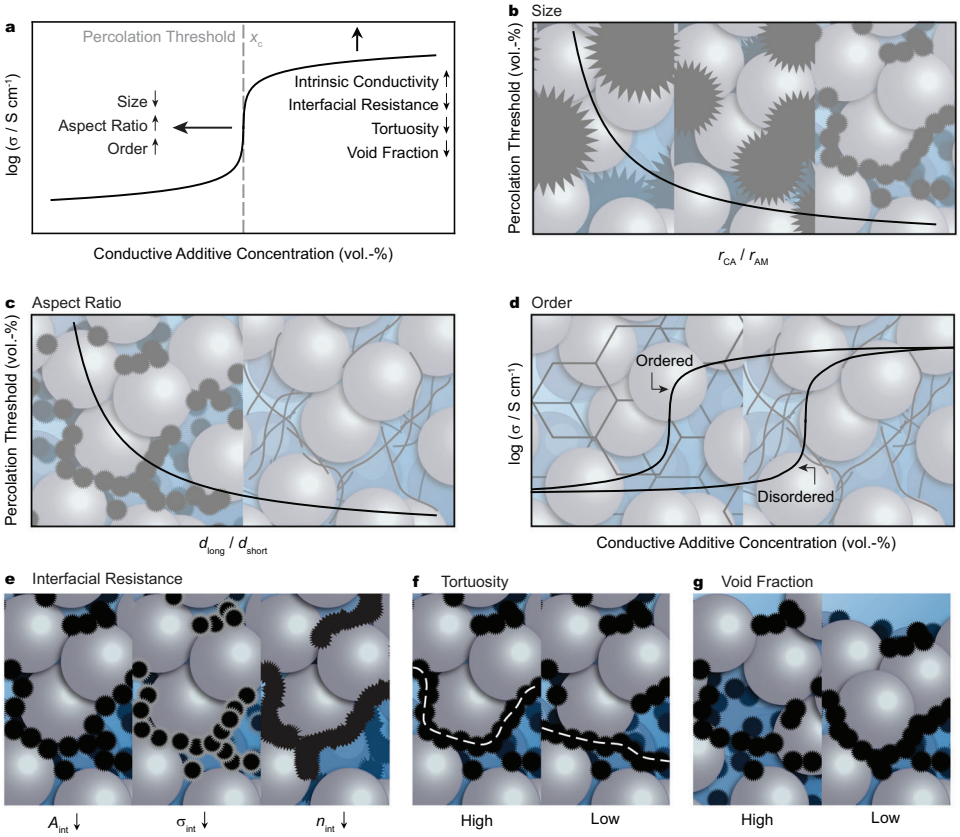

Figure 3. Strategies to lower percolation thresholds and increase long-range electronic conductivity. a) Theoretical percolation curve of the electronic conduction of the composite at various carbon concentrations. b-d) Effect on the percolation threshold of particle size ratio between conductive additive and active material (Graph adapted with permission.[61] Copyright 1993, Elsevier.) (b), aspect ratio of the conductive additive (Graph adapted with permission.[61] Copyright 1993, Elsevier.) (c), and order of the conductive network (Adapted with permission.[62] Copyright 2011, American Chemical Society.) (d). e–g) Effect on the composite electronic conductivity of reduced interfacial resistance (e), tortuosity (f) and void fraction (g).

the conductive additive fills the interstitial space between the active material particles. By restricting the allowed subvolume for the conductive additive to the interstitial space, the effective concentration of conductive additive within this subvolume is significantly increased (Figure 3b).[61,62,64–66] Hence, the overall percolation threshold of the electrode can be lowered significantly. This insight implies that the use of very small conductive additive particles, for instance, CB, can be beneficial in reducing the percolation threshold compared to larger additives like graphite. Similarly, using large active material particles reduces the percolation threshold. This has recently been demonstrated as a viable strategy to reduce the amount of conductive additive for micron-sized Si particle anodes.[67]

Another key insight from PT is that the higher the aspect ratio of the conductive material, the more readily they connect with each other due to the higher excluded volume and the lower the percolation threshold (Figure 3c).[68,69] The percolation threshold is roughly inversely proportional to the aspect ratio of the conductive additive.[61,68,69] This implies that conductive additives like CNTs or graphene lower the percolation threshold significantly compared to spherical conductive additives like graphite or CB.[70]

Thirdly, one can easily verify that the percolation threshold is reduced significantly if the conductive additive is not distributed randomly, but ordered (Figure 3d).[64] For instance, by confining CNTs in a regular hexagonal closed packing, the percolation threshold in a polymer composite can be four times lower than in a randomly oriented sample.[62] Likewise, partially aligned CNTs exhibit reduced percolation thresholds.[64,71] Hence, ordered conductive networks can offer significantly reduced conductive additive contents compared to randomly distributed conductive networks, even though this decrease is not captured by PT, which assumes random distributions.

Although PT is particularly useful for modeling the onset of electronic percolation and how to reduce it, it does not accurately describe conductivity far away from the percolation threshold.[60] PT is also less suitable to describe the factors influencing electronic conductivity above the percolation threshold.

2.3.2. Effective Medium Theory

Instead, EMT based on Newman's porous electrode theory is more frequently used to describe the conductivity beyond the percolation threshold.[72–76] EMT offers an empirically derived approach to describe the influences on electronic conductivity beyond percolation. It also models conductivity as a function of conductive additive content. However, it systematically

Table 1. Characteristics of different conductive additives.[17,39,100,102]

Conductive Additive	Dimensionality	Smallest Dimension [nm]	Aspect Ratio	BET SSA [m^2 g^{-1}]	Conductivity [S cm^{-1}]	Price
CB	0D	10–100	1–10	50	10	$$
SWCNTs	1D	1	100–10000	1.300	10^4–10^5	$$$$$
MWCNTs		5–50	100–10000	200–1000	10^4–10^5	$$$$
VGCF		50–100	250–2000	10–200	10^3–10^5	$$$
Electrospun CF		50–10000	100–1000	10–200	10^2–10^4	$$$
Graphene	2D	<1	250–10000	2.630	10^5–10^6	$$$$$$
RGO		1–5	50–1000	100–500	10–10^2	$$$$$
Graphite	3D	1000	10	5–25	10^4	$

overestimates the percolation threshold,[43] and is therefore more useful to describe electronic conductivity when the conductive additive content significantly surpasses the percolation threshold. According to EMT, the intraparticle conductivity of the conductive network $\sigma_{CN,\,intra}$ can be described as:[77]

$$\sigma_{CN,intra} = \sigma_0^{bulk} \cdot (x \cdot P)^{\mu} \quad \text{where} \quad x = (1-\epsilon) \cdot x_s \tag{3}$$

where σ_0^{bulk} is the intrinsic bulk conductivity of the conductive additive, P is the percolation probability, and related to the coordination number of conductive additive particles.[78] Up until the percolation threshold is reached, it should be 0. μ is the Bruggemann factor, and related to the tortuosity of the conductive path. ϵ is the void fraction inside the electrode and x_s is the volume fraction with respect to total amount of composite material. It follows that reducing the void fraction and tortuosity both improve the intraparticle conductivity within the conductive network (Figure 3f,g).

So far, the influence of interfacial resistance within the conductive network has been neglected. In reality, conductive additive particles never touch each other perfectly, and electrons have to pass between them either via electron tunneling or through highly resistive interfaces (Figure 1).[79,80] For instance, electronically insulating polymeric binder, which is added in practical electrodes to provide mechanical stability, separates out individual conductive additive particles, thereby significantly increasing the interfacial resistance within the conductive network ($\sigma_{CN,inter}$) (Figure 3e).[81,82] The interfacial resistance may dominate over the internal resistance within the conductive additive particles ($\sigma_{CN,intra}$). Instead of adding higher quantities of conductive additive, the overall conductivity may instead be improved by mitigating excessive use of insulating binder, reducing the distance between conductive additive particles through compression, or minimize the total number of contact resistances by choosing conductive additives with larger dimensions.

3. Overview of Carbon Materials

In the previous section, general requirements for the electronic conductivity of conductive additives were reviewed. Apart from that, conductive networks need to be chemically stable, suppress any unwanted side reactions of other battery components, and be mechanically stable to avoid delamination from the current collector. Different materials can be used as conductive additives, e.g. metals,[83] conductive polymers,[84] MXenes,[85–92] or carbon.

Carbon materials are by far the most widely used conductive additive because they are light, (electro)chemically stable, provide good electronic conductivity, and exist in a wide range of structural motifs that can be fine-tuned to suit the needs for a good conductive network.

3.1. Carbon Additives

Over the last decades, numerous carbon materials have been found to be suitable as conductive additives. An overview of the conductive additives discussed in this section is depicted in **Figure 4** and summarized in **Table 1**. They are categorized according to aspect ratio and size into 0D (CB), 1D (CNTs and carbon fibers (CFs)), 2D (graphene), and 3D (graphite).

3.1.1. 0D Materials (Carbon Black)

Carbon Black is a group of carbon materials that is commonly used as a conductive additive because of its good electronic conductivity, very high electrochemical stability, and because it is very cost effective to produce.[13–15] Different CB additives may differ significantly in their properties, such as conductivity, dispersibility in solvents, surface area, size or shape. All of these properties influence the electrochemical performance of the electrode. For this reason, the percolation threshold for CB composites may vary significantly depending on the type of CB and the fabrication process of the composite.[80,103] This diverse set of characteristics is often not appreciated in the scientific literature and papers either incorrectly specify the CB that was used or do not specify it at all.[11,104–116] The aim of this section is therefore to provide a basic understanding of the structure, synthesis, electronic, and chemical properties of CB, as well as an overview of the different types of CB that are available commercially. For a more detailed discussion on the structure and properties of CB, the reader is referred to some excellent reviews elsewhere.[14,117–119]

Structure and Morphology of Carbon Black: Carbon Black is not a distinct allotrope of carbon. Instead, the structure is composed of different regions which correspond to known allotropes of carbon. Carbon allotropes, e.g., graphite, diamond, CNTs, fullerenes, amorphous carbon, etc., differ in how carbon is hybridized within it. The basic bonding modes differ between sp^2 and sp^3, as well as partially hybridized carbon in bent sites for fullerene or CNTs (**Figure 5a–d**).

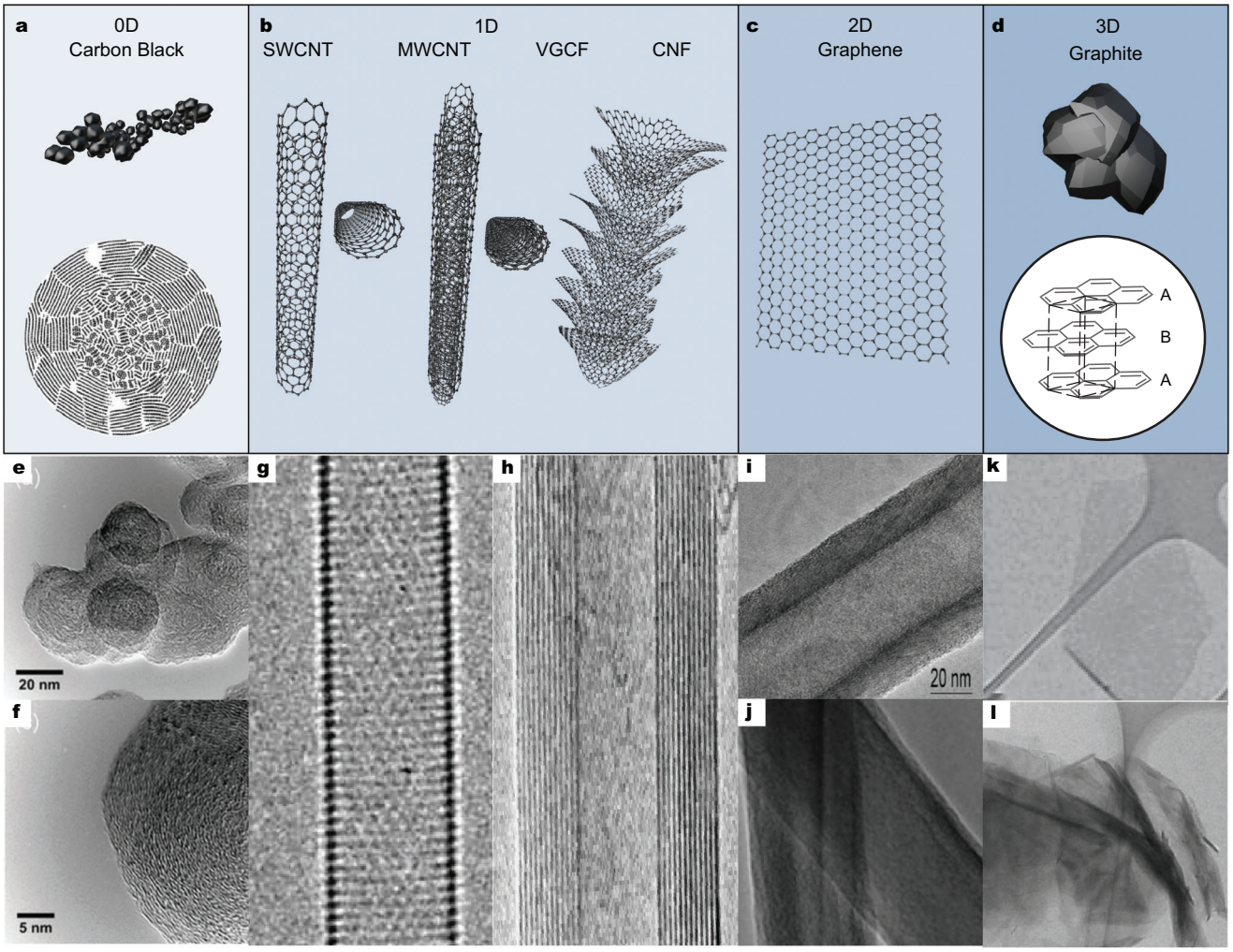

Figure 4. Overview of different carbon conductive additives. a–d) Schematic representation of the structure of CB (Reprinted with permission.[93] Copyright 2011, Elsevier.) (a), Single-walled carbon nanotubes (SWCNTs), multi-walled carbon nanotubes (MWCNTs), vapor-grown carbon fibers (VGCF) and carbon fibers (CFs) (b), graphene (c) and graphite (d). e–l) TEM micrographs of a CB aggregate (Reprinted with permission.[94] Copyright 2015, IOP Science.) (e, f), SWCNT (Reprinted with permission.[95] Copyright 2011, Nature.) (g), MWCNT (Reprinted with permission.[96] Copyright 2002, Elsevier.) (h), VGCF (Reprinted with permission.[97] Copyright 2007, Elsevier.) (i), electrospun CF (Reprinted with permission.[98] Copyright 2009, Elsevier.) (j), graphene monolayer (Reprinted with permission.[99] Copyright 2008, Nature.) (k) and synthetic graphite (Reprinted with permission.[57] Copyright 2011, Elsevier.) (l).

If carbon is sp^2-hybridized, it forms a 2D honeycomb lattice that extends to form an individual graphene layer, as observed in graphene or graphite (Figure 5a,e).[120,121] Carbon atoms inside these graphene layers are characterized by a free p-orbital which forms a delocalized π-orbital over the entire graphene domain. Structural motives with extended, regular sp^3-hybridized carbon form diamond-like domains (Figure 5c,f). In these structures, all the electrons are localized on the carbon atoms and the structure is fully described by covalent bonds without any delocalized electrons.

CB exhibits these two motifs with varying sizes and ratios, both of which influence structure and properties. The ratio of these domains is referred to as the degree of graphitization. It should be noted, however, that CB is amorphous because the size of these domains is smaller than a few nm.[14]

The primary particles (PP) of CB are spherical nanoparticles with thicknesses ranging from 10 to 100 nm (Figure 4a,e,f).[14,117] These PPs feature an amorphous core surrounded by a shell of nm-sized graphene layers.[93,122] The graphene layers stack turbostratically around the amorphous core, resulting in a disordered onion-like nanostructure (Figure 4a,e,f).[93,122,123] The very small size of the CB PPs compared to most cathode active materials makes it a 0D material from the standpoint of PT, and results in very low percolation thresholds.[51,124] However, the point-to-point contact with the active materials may lead to low cross sectional areas for the interface and high interfacial resistances.

The CB PPs fuse together during the synthesis into larger primary aggregates of variable size, ranging from 100 nm to 10 µm, and shape, depending on the exact synthesis conditions. Due to the non-discrete nature of the PPs, separation of individual nanoparticles is impossible without fracturing the primary

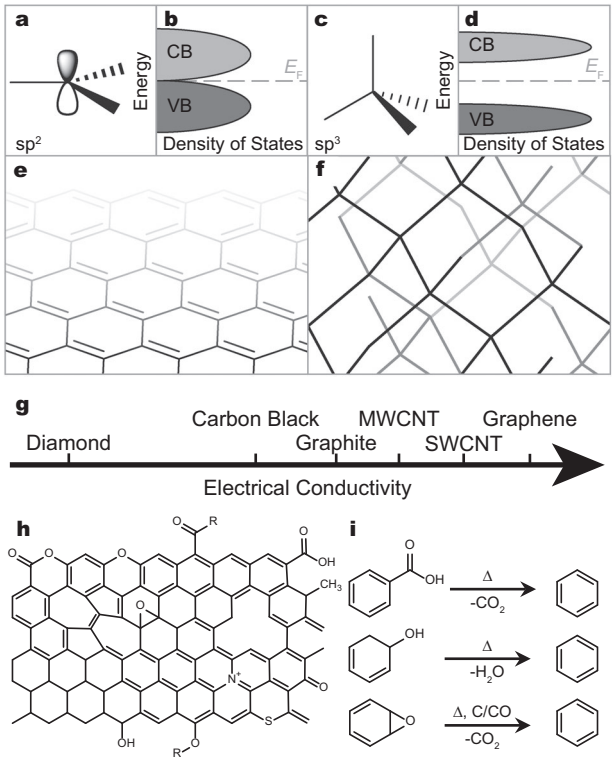

Figure 5. Structure and properties of carbon materials. a,b) Geometry of sp^2-hybridized, (a) and sp^3-hybridized carbon (b). b,d) Simplified band structure of graphene (b) and diamond (d). e,f) Structure of graphene (e) and diamond (f). g) Overview of electrical conductivity of different carbon materials. h) Overview of possible surface functional groups and defects in graphene layers of carbon materials. i) Examples of defunctionalization reactions during heat treatment of carbon materials.

agglomerate.[14,119] Importantly, the morphology and size of these aggregates play a pivotal role in determining various properties, including electronic conductivity, and are therefore important characteristics to distinguish different CB materials.[14] For instance, CB with high aspect ratio aggregates (up to 10) are desirable for low percolation thresholds. While the size of the primary aggregates can be measured from transmission electron microscopy, aggregate size is normally measured indirectly by Brunaue-Emmet-Teller (BET) specific surface area (SSA), which is inversely related to CB aggregate size. While the inner porosity of the PPs and aggregates can also affect the surface area, this effect is usually negligible for CB with surface areas less than 100 $m^2\ g^{-1}$.[57]

Lastly, the primary aggregates can agglomerate to larger micron-sized secondary particles. These agglomerates significantly influence electrode preparation, which is discussed in Section 4.1.

Electronic Conduction in Carbon Black: Electronic conduction in CB occurs by two main mechanisms. First, the graphene layers on the PP surface are highly conductive because they are zero-bandgap semiconductors (Figure 5b).[14,125,126] In other words, highly mobile electrons can travel in the delocalized π-orbitals of the graphene layers. Consequently, CB containing a high number of graphene layers, i.e., a high degree of graphitization, is more conductive.[127] Higher conductivities are also expected for CB with small PPs and correspondingly high surface area, composed of graphene layers.[124]

Second, electrons are conducted between graphene domains or between carbon particles through tunneling on a sub-nm length scale.[14,50,80,124] These tunneling events occur frequently in CB because of the very small graphene layer size. The interfacial resistance associated with electron tunneling often dominates over the internal resistance in the graphene domains. CB therefore has the lowest conductivity of the conductive additives discussed in this review (Figure 5g). Having intimate contact between CB PPs, e.g., through compression, is crucial to increasing the cross sectional surface area between particles and aggregates.[80,103]

Likewise, larger graphene domains reduce the number of interfacial contacts within a given distance and therefore reduce the resistance of CB (Figure 3e). Crystallization of these domains to larger sizes is a viable option to improve electronic conductivity. However, complete graphitization of CB is not possible due to the highly strained turbostratic stacking of the graphene layers.[117]

As for the electronic structure of the CB core, it exhibits large regions of sp^3–hybridized carbon. Electrons in these diamond-like domains are localized at the carbon center and are therefore non-conductive (Figure 5d). Likewise, the introduction of sp^3–hybridized carbon into the graphene layers on the PP surface, either through deliberate chemical functionalization, or because of the unwanted presence of residual surface functionalities, disrupts the π-orbitals and localizes the electrons on the carbon center, thereby reducing electron mobility.[126–128]

Because electronic conductivity and percolation thresholds are so sensitive to PP size, aggregate size, aggregate morphology, carbon purity, degree of graphitization, and contact between particles, the observed percolation thresholds and electronic conductivities reported in the literature vary widely.[80,124] CB with branched or linear aggregates typically exhibit significantly lower percolation thresholds than spherical CB aggregates,[80] and percolation thresholds as low as 0.6 wt.-% in polymer composites can be achieved.[129] Similarly, compression[103] and graphitization improve the electronic conductivity.

Synthesis of Carbon Black: Carbon Black is synthesized from the gas phase via the thermal decomposition of hydrocarbon precursors. Decomposition and carbonization occur either under i) heat treatment in a partially oxygen-depleted atmosphere or ii) a fully oxygen-depleted atmosphere (pyrolysis).[14,119,130] In the first case, the hydrocarbon-rich feedstock is co-injected with air to partially combust the carbon and generate the required heat. At temperatures above 1000 °C, cracking of the precursors occurs, and the uncombusted feedstock decomposes to form CB.

While the exact mechanism of CB formation during thermal decomposition is not yet fully understood, it is acknowledged that PP nucleation, particle growth, and aggregation all happen during this step.[131–135] Hence, the exact conditions during thermal decomposition influence the CB PP size, aggregate size, and shape, and therefore the physicochemical properties.

Depending on the synthesis conditions, heteroatoms are eliminated from the carbon precursor at these elevated temperatures to reach final products with >97 to >99.9 wt.-% carbon content.[117,119] High-quality CB with very high carbon contents is required for good conductivity and low impurity levels. For

electrode preparation, conductive CB is used.[57] Because of the variable conditions and possible feedstock, a plethora of different CBs is produced by this method, from furnace black used in the rubber industry to battery-grade Super and ENSACO CB.[15,119,130,136]

Alternatively, heat treatment can be done under the complete exclusion of air, known as the thermal black process.[117] This process employs lighter, gaseous hydrocarbons. Instead of generating the required heat for hydrocarbon cracking by partial combustion, it is generated in a separate step by burning some of the hydrocarbon first, and then injecting a fresh batch of hydrocarbon into the heated furnace chamber.[117] A special case of this process is the acetylene process, where no separate heating step is required because the combustion proceeds autogenously above 800 °C.[119,136]

Surface Chemistry of Carbon Black: Carbon itself is one of the most (electro)chemically stable materials and therefore attractive for battery applications.[117] Nevertheless, its reactivity is enhanced at the surface of the carbon material, especially at sites with unsaturated valences, for instance edge sites or basal plane defects (Figure 5h). In order to terminate edge sites and basal plane defects, carbon reacts with the surrounding atmosphere, leading to the introduction of various surface functional groups, e.g. hydrogen, sulfur, nitrogen and most often oxygen-containing groups, such as carboxylic acids, carboxylic anhydrides, lactones, lactols, phenolic hydroxyls, carbonyls, o-quinones, or ethers (Figure 5h).[137,138] These surface functional groups are more reactive than defect-free carbon.[139,140] They are therefore important for chemically and electrochemically induced side reactions during cell operation (see section 4.4).[139,141,142] For instance, electrolyte decomposition can occur due to the presence of surface functional groups, thereby reducing the cycling stability.[143,144]

As previously discussed, surface functional groups also reduce the electronic conductivity of CB.[126,128] Generally, the lower the number of heteroatom impurities, the higher the electronic conductivity, as heteroatoms perturb the sp^2-hybridized graphene-like domains within the CB PPs. Hence, defunctionalization as a form of purification is required for battery-grade CB. Thermal treatment is the preferred purification method in industry because CB synthesis already occurs at high temperatures, so no subsequent treatment steps are required. In a partially or fully oxygen-depleted atmosphere, heteroatoms are eliminated and the overall carbon content of the material increases. Elimination reactions yield sp^2-hybridized carbon, so electronic conductivity is improved by this strategy (Figure 5i).

However, retaining some amount of functional groups may be desirable to adjust the polarity of the carbon additive. Highly pure CB is apolar, while active materials like LFP, NMC and LCO are polar due to their ionic nature. Likewise, organic solvents used in electrode preparation are polar. This polarity mismatch may hinder dispersion during slurry preparation or cause phase separation during subsequent drying, both of which can result in overall poor electronic networks. Similarly, a polarity mismatch with the electrolyte may result in poor wettability of the carbon conductive network. The amount of functional groups in commercial CB is mainly controlled by the heat treatment step. However, subsequent chemical treatments can be applied to introduce additional functional groups. For an in-depth discussion of different functionalization methods of CB, the reader is referred to an excellent recent review by Andreoli et al.[14]

Overview of Commercial Carbon Blacks for Lithium-Ion Batteries: CB is used primarily in the rubber tire industry, but its properties make it very appealing for electrochemical applications as well, like supercapacitors,[145,146] fuel cells,[147–150] photocatalysts,[151] or batteries.[14,21,41,57,81,94,143,152–177] In this section, we only present an overview of conductive CB with high purity levels because they are required for battery applications.[57] To achieve low percolation thresholds, battery-grade CB displays large complex aggregates with high aspect ratios.[119] Their large size also minimizes the number of interparticle contacts and thereby reduces interfacial resistances. The complex aggregate structure is also beneficial for electrolyte uptake in the final electrode.

A list of commonly used CBs is provided in **Table 2**. Examples of battery-grade CB include special furnace blacks like Super P,[57,94,153–163] C-NERGY Super C65,[21,41,57,81,143,163–170] and C45,[57,178] and Super S,[57,82,179,180] as well as acetylene blacks like Denka Black,[57,171–177] Ketjenblack,[164,172,181–183] and Shawinigan Black.[153] Most CB products exhibit surface areas below 100 $m^2\ g^{-1}$, corresponding to PP sizes between 30 to 40 nm.

While all of these CBs exhibit very high electronic conductivity relative to other CBs, e.g. those used in the rubber industry, their conductivity in composites can still differ by over an order

Table 2. Commercial conductive carbon black materials used in LIBs.[14,15,57]

Process	Manufacturer	Commercial Name	BET SSA [$m^2\ g^{-1}$]	PP size [nm]	Conduc-tivity	Disper-sibility	Purity	Refs.
Partial Combustion	Imerys	Super PLi	62	30–35	++	+++	+++	[57,94,153–163]
		C-NERGY Super C65	62	30–35	++	+++	++++	[21,41,57,81,143,163–170]
		C-NERGY Super C45	45	35–40	+++	+++	+++	[57,178]
	Timcal	Super S	50	35–40	+	++	+	[57,82,179,180]
Acetylene Process	Denka Corporation	Denka Black Li	68	35	+	++	+++	[57,171–177]
		Ketjenblack EC300J	800	79	+++	+	++	[172,181,182]
	AkzoNobel	Ketjenblack EC600JD	1270	68	++++	+	++	[164,172,183]
	Chevron Phillips	Shawinigan Black	75	42	+	+	+	[153]

of magnitude. For instance, Spahr et al. measured the electronic conductivity of various CBs in LCO/CB composites with 3 wt.-% CB prepared by dry mixing.[57] The measured conductivities differed significantly between different CB with 0.002 S cm^{-1} for Super S, 0.01 S cm^{-1} for Denka black, 0.02 S cm^{-1} for Super P Li and Super C65, and 0.1 S cm^{-1} for Super C45. As previously discussed, the conductivity of the composite improved upon compression due to the increased volumetric CB concentration and the larger cross sectional area between CB particles. The authors attributed the different conductivities of the composite at low carbon contents mainly to the different carbon distribution as a result of composite preparation, as opposed to differences in intrinsic conductivity. In particular, Super C45 showed high conductivity in the composite despite lower degrees of graphitization. This was attributed to the excellent dispersibility of Super C45 with polar LCO, due to the relatively high amount of carboxylic and oxygenated functional groups in Super C45 compared to other battery-grade CBs. To illustrate this, the authors prepared composites with the same carbon content by wet mixing. Consequently, the dispersion of CB was improved and the conductivity increased three times for Super C65 CB.

Lastly, it should be noted that the carbon content of battery-grade CB is not only dependent on the amount of surface functional groups, but also on the amount of metallic residues from the synthesis process.

3.1.2. 1D Materials

Carbon Nanotubes and Carbon Fibers are highly desirable conductive additives due to their very high aspect ratios, which can significantly lower the percolation thresholds compared to CB or graphite.[16,18,184–187] They are often considered 1D materials because of their small diameter and high aspect ratio (Figure 4b,g–j)

Carbon Nanotubes: Discovered in 1991,[188] CNTs are another commonly used conductive additive that is particularly attractive due to their high electrical and thermal conductivity, mechanical stability, and tunable surface functionality.[184] Their use for electrochemical applications has therefore been a subject of active scientific research and many excellent reviews have been published on their various use cases.[16–18,184,185,189–191]

CNTs consist of slightly pyramidalized sp^2-hybridized graphene layers where the basic hexagonal honeycomb structure is wrapped into a 1D tubular structure.[17] The diameter of CNTs can vary between 1 to 100 nm, while their length can reach several mm.[192] Hence, they exhibit a high aspect ratio of up to 10000,[193] and high surface areas of up to 1300 m^2 g^{-1}.[17] Depending on the number of graphene layers stacked on top within the tubular structure, CNTs are classified into single-walled CNTs (SWCNTs) and multi-walled CNTs (MWCNTs).[17] SWCNTs have diameters of 1 to 10 nm, while MWCNTs can reach up to 100 nm in diameter. Owing to their hollow structure, a unique feature of CNTs compared to other carbon conductive additives is their ability to confine active materials within the CNTs.[194–198] This can be advantageous for active materials that exhibit significant volume changes, as discussed in Section 5.

CNTs are mainly synthesized by two different processes: i) sublimation of graphite at very high temperatures (up to 4.000 °C), typically generated in electrical arcs,[199–201] or through laser ablation,[202] and ii) pyrolysis of carbon-containing compounds.[192,203] The decomposition of gaseous products through chemical vapor deposition (CVD) is most commonly used to obtain large quantities of CNTs at moderate temperatures (500 to 1300 °C).[203] These processes enable the growth of CNTs with extremely high purity and very few surface functional groups. MWCNTs are much easier to produce on large scales than SWCNTs,[17] so most battery applications employ MWCNTs. However, even MWCNTs are significantly more expensive than most CBs and are so far only used in specialized high-power batteries or for lab-scale applications.

Due to their high purity and very large size of unperturbed graphene-like domains, CNTs exhibit extremely high electronic conductivities on the order of 10000 S cm^{-1}.[189] Moreover, the observed percolation thresholds are significantly lower than for CB due to the very high aspect ratio.[51–53,204–206] However, the experimentally reported percolation thresholds for CNTs can vary widely, depending on the aspect ratio and dispersion state of the CNTs.[207] For aligned MWCNTs in epoxy-resins, percolation thresholds can be as low as 0.0025 wt.-%.[51]

The surface structure of CNTs is comparable to that of the graphene domains in CB (Figure 5h). While the amount of functional groups compared to the total carbon content is much higher in CNTs than for most CB, it is important to remember that CNTs have much higher surface areas and a better comparison of carbon purity might be the density of functional groups per surface area.

CNTs can be readily functionalized, e.g. through the introduction of hydrophilic functional groups,[208,209] or nitrogen doping.[210] For in-depth reviews of different functionalization methods of CNTs, the reader is referred elsewhere.[17,211–213] This review focuses on relevant functionalizations for battery applications. For instance, functional groups on CNT can be used as anchoring points for the synthesis of active materials.[209] Functionalization, e.g. via carboxylation, may also help improve dispersibility in the presence of polar active materials like LFP and NMC.[208] However, the reduced electronic conductivity caused by functionalization can outweigh the benefits of this strategy.[208]

An important consequence of CNT functionalization is that redox-active functional groups can cause additional capacity or pseudocapacitance.[214] The reversible capacity for CNTs as active materials may vary hugely.[189] They do not exhibit a pronounced voltage plateau and have very poor coulombic efficiency. This excludes them as viable active materials, but nevertheless needs to be considered when using them as conductive additives.

Carbon Fibers: In this section, we discuss two types of carbon nanofibers, which are distinguished by their synthesis method: i) vapor-grown CFs (VGCF) and ii) electrospun CFs (Figure 4b,i,j). Both VGCF and electrospun CFs have found application as conductive additives and the reader is referred to excellent reviews for a more in-depth treatment.[17,186,187,215–217]

Just like CNTs, VGCF is synthesized via a CVD process.[217,218] They were historically discovered much earlier than CNTs. Compared to CNTs, VGCF typically exhibits larger fiber diameters, around 50 to 200 nm, as well as wall thicknesses of 10s of nm.[219] VGCF also exhibits turbostratic graphene layers of much smaller lateral dimensions than in CNTs, which are interrupted by amorphous carbon domains.[17] Similarly, the stacking of the graphene layers exhibits a larger disorder than in MWCNTs.

Correspondingly, VGCF has lower surface areas (10 to 200 m^2 g^{-1}), lower aspect ratios (250 to 2000),[219] as well as slightly lower electronic conductivities (10^3 to 10^5 S cm^{-1})[100] than CNTs. The price of VGCFs is 2 to 3 times lower than for MWCNTs because the synthesis of VGCF can tolerate larger amounts of impurities than the growth of CNT.[219] Compared to other conductive additives, the very low surface areas, as low as 10 m^2 g^{-1}, make VGCF an attractive conductive additive for applications where side reactions within the electrode need to be suppressed as much as possible. For instance, VGCF has been used in commercial high-power batteries,[220,221] despite its higher price than CB.

Electrospun CFs have been known since the 1960s.[217] The fiber diameter can vary between 10s of nm to a few µm. Contrary to VGCF, electrospun CFs are not hollow. CFs are prepared from a viscous polymer solution with a carbon precursor, e.g. include polyacrylonitrile (PAN), polyimide, polyvinyl alcohol, polyvinylidene difluoride (pVdF) or pitch, and a sacrificial polymer.[215,217] The polymer solution is then ejected from a needle at a high voltage onto a heated substrate, where the solution evaporates, and the precursor is subsequently carbonized at high temperatures. Carbon purity and electronic conductivity are primarily dependent on the precursor and carbonization temperature.

3.1.3. 2D Materials (Graphene)

Graphene is the prototypical building block that facilitates the electronic conduction in all carbon additives.[121,222–225] Theoretically, it should be just a single-layer thick with a very high theoretical surface area of 2630 m^2 g^{-1}.[226,227] Practically, it is often 2 to 10 layers thick. Beyond this thickness, its electronic properties become indistinguishable from graphite, which is discussed separately in section 3.1.4.[222] Graphene is a 2D material due to its extremely high aspect ratio and thinness and offers area-to-point contacts with active materials. Many reviews have been published on the use of graphene for electrochemical energy storage applications.[16,19,20,127,184,228–231]

Graphene sheets can vary in lateral dimensions between less than 100 nm (nanosheets), up to 10s of µm (microsheets).[120] Their very high aspect ratio enables the formation of a conducting composite polymer at percolation thresholds below 0.1 vol.-%.[232,233] In addition to aspect ratio, the size ratio between conductive additive and active material is very important for the observed percolation thresholds, as discussed in Section 2.3.1. Graphene stands out in this respect, with lateral size dimensions comparable to active materials, e.g. LFP. The large lateral dimensions are also important for the conductivity on short-range scales, as discussed in Section 2.1. Due to its structural flexibility, graphene can adopt different structural modes and contact with the active material depending on the size of graphene, as well as the size of the active material.[160,234] This has important implications for the electrochemical performance discussed in Section 4.2.2.

Graphene can be synthesized by several different methods:[19,121,224,225,235] i) exfoliation from graphite,[99,236] ii) epitaxial growth on top of another crystal,[237] iii) unzipping of MWCNTs,[238,239] or iv) reduction of graphene oxide (GO) to reduced GO (RGO).[240–242] The synthesis of RGO is the only commercially relevant synthesis of graphene.[127] For this reason, the vast majority of battery research on graphene also uses RGO.[156,157,243–246] Its synthesis is therefore discussed further. In the initial step, highly pure graphite oxide is obtained via oxidation of graphite using a modified Hummer's method.[247–249] Due to its large number of hydrophilic functional groups, graphite oxide is easily dispersible and can be exfoliated via ultrasonication to obtain GO sheets in large quantities. Lastly, the exfoliated GO is reduced to obtain RGO.[240–242] Reduction can occur chemically, thermally, electrochemically or by a combination of the above, although thermal reduction is most often used.[224,225] The obtained RGO is typically several layers thick and usually has oxygen contents above 5 to 10 wt.-%.[102,224] Although more feasible than the alternative routes for obtaining graphene, the costs of graphene are still one order of magnitude higher than for MWCNTs.

While the reduction of GO is suitable to obtain larger quantities of RGO, the residual functional groups on the surface reduce the electronic conductivity of the obtained graphene. Without reduction, the GO precursors are an electronic insulator due to the disrupted π-orbital.[223] Moreover, the harsh conditions for exfoliation and reduction result in small flake sizes of only a few hundred nanometers,[225] as well as significant porosity within the resulting flakes. Interflake resistance must therefore be considered when measuring the electronic conductivity of RGO composites. As a result, RGO is typically less conductive than CNTs, with reported conductivities for polymer composites or electrodes ranging from 10 to 100 S cm^{-1}.[224] Importantly, the ability to vary the polarity of graphene by going from GO to RGO is sometimes exploited in electrode preparation. For instance, polar GO is often mixed with the active material to obtain well-dispersed slurries. Heat treatment then reduces GO to obtain electronically conductive RGO in a subsequent step.[250]

Graphene can be chemically modified, similar to other carbon conductive additives.[121,224,225,251,252] Common strategies involve heteroatom doping, e.g. nitrogen doping, or oxidation to introduce hydrophilic surface groups.[252–254] While these functionalizations generally reduce electronic conductivity, they may help to improve contact with the active material.[255] Functional groups can also serve as anchors for the synthesis and growth of nanoparticulate active material on top of the graphene.[245,256] Similarly, functional groups or nitrogen doping can also help with anchoring polysulfides in Li-S batteries and can therefore be used to enhance the cycling stability of sulfur cathodes, as discussed in more detail in Section 5.2.[110,257–261]

Lastly, it should be mentioned that similar to CNTs, the very large surface area of graphene and, subsequently, of functional groups leads to large observed (pseudo)capacities or -capacitances.[184,234] This needs to be considered when assessing the charge-storage capacities of active materials, as well as the overall electrochemical stability of electrodes.

3.1.4. 3D Materials (Graphite)

Graphite is one of the chemically stable, crystalline allotropes of carbon. While graphite is typically known as the anode active material in LIBs, it is also used extensively as a conductive additive.[57,81,153,156,157,262] Conductive graphite enhances the

electrode conductivity and differs structurally from electrochemically active graphite.

Graphite consists of very large domains of periodically stacked graphene layers (Figure 4d). Thermodynamically stable graphite has a hexagonal crystal structure, with a stacking order of ABABAB (H2) and an interlayer spacing of 0.3354 nm,[263] although a rhombohedral modification also exists with an ABCABC (R3) stacking order.[264] Similarly, stacking faults are described by the rhombohedral modification, but these stacking faults can be alleviated by heat treatment to convert back to the hexagonal crystal structure.[15] The degree of crystallinity dictates the electronic conductivity, so only highly crystalline graphite is used in battery applications.[15]

The most common shape of graphite particles is flake-like. Graphite flakes are polycrystalline and often exhibit a plate-like shape (Figure 4d,l).[15] The crystalline domains in these flakes exhibit varying degrees of preferred orientation, i.e., texture. The larger the aspect ratio of the flake, the higher the degree of preferred orientation of the crystalline domains within. The size of the graphite flakes can vary, depending on the graphite source and history, but the graphite used in battery applications is typically less than 10 µm in diameter. The larger size of graphite compared to smaller sized conductive additives like CB implies higher percolation thresholds, which is also experimentally observed.[57]

Because of the very high purity that can be achieved within the graphene layers of graphite, the electrical conductivity can exceed 30000 S cm^{-1} along the graphene layers.[15] Hence, graphite exhibits higher intrinsic conductivities than CB, although at significantly higher carbon contents. However, the through-plane conductivity is only on the order of 1 S cm^{-1}.[265] Likewise, graphite exhibits extremely high thermal conductivity, which is relevant for thermal management in commercial high-power batteries.

Diverse graphite products are commercially available. They differ in size, shape, surface area, and purity. An overview of commercial graphite materials can be found in **Table 3**.

Battery-grade graphite is either obtained i) by synthesis or ii) from natural graphite after purification.[15,130] Synthetic graphite is synthesized from carbon precursors like petroleum cokes or coal tar-based cokes.[136] The amorphous coke precursors are then crystallized under exclusion of O_2 at temperatures above 2500 °C to obtain graphite. Heating may be applied by joule heating with an electric current, e.g. in the Acheson furnace technology.[136] By controlling the purity of the precursor coke, the final product may reach carbon contents beyond 99.9 wt.-%.[15] In a last step, the as-synthesized graphite is mechanically treated by grinding and sieving to obtain the desired particle size. All of the graphite materials shown in Table 3 are synthesized by the Acheson technology.[57]

Alternatively, natural graphite can be purified from graphite ore by flotation processes.[15] Because of the relatively large size of the natural graphite particles and little porosity within the graphite, its surface area is typically much smaller than for other carbon additives. Hence, there are also less surface functional groups that need to be considered for possible side reactions. Nevertheless, thermal treatment around 1500 °C is often subsequently applied to reduce the number of surface functionalities of the natural graphite particles and thereby reach the desired carbon content.[130]

Table 3. Commercial graphite materials from Imerys used as conductive additives.[15,57]

CB Grade	Commercial Name	Particle shape	BET SSA [m^2 g^{-1}]	d_{90} [µm]
TIMREX	KS4	Isometric irregular spheroids	26	4.8
	KS6	Isometric irregular spheroids	20	6.5
	KS15	Isometric irregular spheroids	12	17
	SFG6	Anisometric flakes	16	6.5
	SFG15	Anisometric flakes	7	18
	SFG44	Anisometric flakes	5	48
	MX15	Strongly Anisometric flakes	9	18
C-NERGY	KS6L	Isometric irregular spheroids	20	6.5
	SFG6L	Anisometric flakes	17	6.5

3.2. Carbon Coatings

The last type of carbon materials that is reviewed here are carbon coatings. Carbon coatings reduce the electronic diffusion lengths in the non-conductive active material, e.g. LFP, and provide good electronic contact with the active material (Figure 1e).[266–268] They therefore reduce the overall resistance by reducing R_{AM} and R_{int}. Hence, carbon coatings are widely applied in academia and industry. In this section, we discuss the structure, morphology, and synthesis of carbon coatings primarily for LFP containing cathodes.[182,269–273] However, carbon coating has also been applied to cathodes containing LCO,[274,275] or NMC.[276]

Industrial carbon coatings for LFP are typically uniform coatings with 1 to 2 nm thickness and high degrees of graphitization, i.e. high amounts of graphene domains through which electronic conduction occurs rapidly.[266,268,269] At the same time, carbon coatings exhibit a certain degree of porosity in the amorphous regions, which provide access for Li-ions to diffuse through the coating layer. The precise structure of the carbon coating, i.e. coating thickness, degree of graphitization, coating uniformity, and morphology, are determined by the synthesis precursors and conditions. Carbon coatings can be formed directly during the synthesis of the active material or in a subsequent step.[266] Industrially, a two-step process is usually preferred because the separation of the two processes allows more control in each step over the desired properties, i.e. high-quality LFP in the first step and high-quality coating in the second step. As with the synthesis of CB, carbon coatings are synthesized under inert conditions at temperatures between 600 to 800 °C, by pyrolyzing carbon-containing organic precursors mixed with the active material.

Typical precursors are various sugars, e.g. glucose,[277] and sucrose,[277,278] carboxylic acids like citric acids,[270,272,279] or carbonaceous polymers.[269,271,280,281]

The degree of graphitization is controlled by the choice of precursor and the sintering temperature.[268] Sucrose,[282] and polyaromatic polymeric precursors[269,271] can form highly graphitic carbon coatings. Higher synthesis temperatures improve graphitic contents. However, just like with CB, the synthesis temperatures are usually too low to allow full graphitization, which only occurs at temperatures above 2000 °C. The coating thickness is mostly determined by the amount of carbon precursor, the surface area of the active material, the porosity of the coating and the degree of carbonization, which is, in turn, determined by process conditions such as heating temperature and time.[266,272] Finally, the coating porosity also depends on the precursor. Overall, sugar is the preferred precursor for commercial LFP coatings because of its ability to provide high-quality carbon coatings with high degrees of graphitization, good porosity, and its abundance and therefore, cost-effectiveness.[266]

It is important to keep in mind that pyrolysis of hydrocarbons generates a reducing atmosphere. Active materials can therefore easily be reduced carbothermally during carbon coating under these atmospheres and temperatures.[283] Pyrolysis is, consequently, not suitable for all active materials and process parameters may have to be adjusted to minimize side reactions. However, high-quality carbon coatings cannot be obtained by low-temperature coating strategies so far.

4. Conductive Networks in Electrodes with Commercial Active Materials

In this section, the construction of effective conductive networks in electrodes with commercial active materials, such as NMC, LCO, LFP, or Lithium nickel cobalt aluminum oxides (NCA) are reviewed. Because of the strong focus on commercial applicability, the material and electrode requirements mentioned previously apply strictly, i.e. cells are optimized for energy and/or power density and high cycling stability. To meet their performance requirements, conductive additive contents only slightly above the percolation thresholds are used, typically below 2 wt.-% for state-of-the-art electrodes.[13] The precise amount depends on the type of carbon conductive additive, and active material, as well as their particle size distributions.[15] At such low conductive additive contents, certain problems arise that are often neglected in academic research. For instance, proper electrode preparation becomes crucially important to distribute the conductive additive homogeneously within the composite electrode.[284] Important aspects about electrode preparation from wet mixing/coating, and how the processing parameters affect the structure and properties of the conductive network, are therefore discussed in Section 4.1.

The final microstructure of the conductive network, and therefore the long-, medium-, and short-range scale, is crucially dependent on the types of conductive additives.[167] The choice of conductive additive also dictates the pore size within the resulting electrode, which is relevant for ionic conductivity. Because of its lower density compared to the active material, CB occupies a significant volume of the electrode and therefore influences the electrode microstructure significantly.[285] For instance, as much as half of the porosity filled by electrolyte is determined by the conductive additive.[285] Hence, choosing the right conductive additive dictates the microstructure and tortuosity for Li-ion diffusion.[40,161,286]

High-energy and high-power electrodes have diverging performance limiting factors, as recently highlighted by Nirschl et al.[287] Consequently, there is not one optimal conductive network structure for high-energy and high-power electrodes because of the tradeoffs that arise from optimizing either electronic or ionic conductivity.[288,289] Strategies for conductive networks for high-energy and high-power electrodes are discussed separately in Sections 4.2 and 4.3. Both the structure of state-of-the-art commercial conductive networks are discussed, and emerging strategies are reviewed that might become commercially viable in the future. Finally, the influence of the conductive network on cycling stability is discussed in Section 4.4.

4.1. Preparation of Conductive Networks

Battery electrodes need to be fabricated from the individual constituents. The best hypothetical conductive network is therefore of little use if it cannot be processed into a working electrode. Commercial batteries consist of thin electrode films of about 50 to 100 µm thickness. The electrodes are fabricated by first dispersing all the electrode ingredients, i.e. active material, conductive additive, and binder in a solvent.[22,290,291] The viscous slurry is then ball-milled or knitted to form a well-mixed dispersion. The dispersion is then printed or coated onto the current collector. Finally, the coated electrodes are dried to remove the solvent. A final calendaring step is usually applied to increase the electrode density and improve the electronic contact inside the electrode, as well as adhesion with the current collector. All of these steps affect the final electrode performance, so precise control over each step is crucial.[166,171] While other methods for electrode preparation exist, this is the dominant preparation process used in academia and industry across different TRL levels. In the following, we discuss the different steps, and summarize how each parameter affects the conductive network. For a more in-depth analysis, the reader is referred to some excellent reviews on the detailed processing conditions required for state-of-the-art electrodes.[13,290–293]

4.1.1. Wet Mixing

Commercial cathode slurries are prepared with N-Methylpyrrolidone (NMP) as solvent and pVdF as binder. The wet mixing process plays a pivotal role in controlling the degree of dispersion and deagglomeration of all components, including the active material, binder, and conductive additives.[13] Various techniques can be applied for dispersing, characterized by direction, compression, shear stress, etc. Hydrodynamic shear mixing and ball milling are the most commonly employed mixing methods.[290] The amount of free solvent relative to solid content dictates the slurry viscosity. CB can take up significant amounts of solvent within the primary aggregates and secondary agglomerates, reducing the amount of free solvent. More solvent is therefore required to achieve the desired viscosity, driving up

solvent consumption and production cost.[294–296] Meanwhile, graphite takes up significantly less solvent because of its lower surface area and porosity. Its impact on rheology is therefore negligible in comparison.[166]

The rate of shear mixing controls the degree of deagglomeration in CB during wet mixing, which directly affects both the morphology of CB and the resulting network, as well as the CB dispersion in the electrode. How much deagglomeration of CB is desired is not straightforward to answer. On the one hand, deagglomeration is crucial to allow homogeneous carbon distribution within the entire electrode to ensure good conductivity on medium-range scales and high surface coverage of the active material.[287,297,298] This is especially important at the very low carbon contents used in industry. Deagglomeration also increases the amount of free solvent and thus lowers the slurry viscosity.[13] Because of this, the conductive additive is often pre-dispersed in NMP.[57,170,181] Subsequently, the active material is added and a homogeneous dispersion at higher solid contents can be achieved. For commercial applications, reducing the amount of solvent for slurry preparation is crucial to lower process energy consumption and overall cost, especially because of the health hazards associated with solvents like NMP. Dry or low solvent processing techniques are therefore being investigated.[293]

On the other hand, excessive deagglomeration may also not be desirable. Due to the presence of binder in the slurry, a thin layer of binder covers all non-continuous surfaces in the slurry during electrode drying, leading to an insulating layer on the conductive additive surface.[81,82] Likewise, minimizing the surface of CB on which binder can deposit is important.[166,299] For this reason, lower surface area CBs with larger aggregate sizes, e.g. Super P, Super C65, and Super S are employed in industry. Wet mixing needs to preserve some of the CB aggregates to retain fast electronic conduction within them.[81,166,299] Minimizing binder usage also reduces the negative impact on electronic and ionic conductivity, but may negatively affect mechanical stability. Choosing the right ratio of conductive additive to binder is therefore crucial.[174–177,300] Moreover, completely deagglomerated CB cannot form a gel-like network to stabilize the active material upon drying.[162] Instead, CB migrates during drying, resulting in inhomogeneous conductive networks and ultimately poor rate capability.

Overall, some degree of deagglomeration may be needed for good conductivity on the short- and medium-range scales. However, the conductivity on long-range scales can be deteriorated by deagglomeration. Consequently, the precise degree of deagglomeration needs to be determined for every individual system, depending on the choice of conductive additive, active material, binder, and their relative amounts.

4.1.2. Dry Mixing

A preliminary dry mixing step of conductive additive and active material in the absence of binder can enable intimate contact between the two components and good surface coverage of the active material. When the insulating binder is added during wet mixing, the intimate contact between active material and conductive additive can be retained during subsequent wet mixing and the binder cannot precipitate at the interface during drying. This can significantly reduce the interfacial resistance in the final electrode,[21,81,159] and subsequently improve the rate capability observed at commercial areal loadings and carbon contents.[21]

Dry mixing may also partially deagglomerate the CB, resulting in more free solvent in the subsequent wet mixing step and allowing for higher solid contents in the slurry.[262] However, excessive dry mixing can fracture the CB primary aggregates and thereby reduce the structural benefits of the CB primary aggregates on electrolyte uptake and electrical conductivity.[301] Moreover, such excessive ball milling increases the CB surface area, which is an important parameter for cycling stability, as discussed in Section 4.4.[14]

4.1.3. Slurry Coating

After the desired slurry is obtained, it is coated onto Cu or Al metal foils. The shear rates applied during coating are typically lower than during mixing.[13] Industrially, slot-dies with shear rates of 10 to 30 m min^{-1} are applied, whereas academic research typically uses rates of 1 to 2 m min^{-1}. Shear rates can influence the electrode microstructure and porosity, as well as the ordering of the conductive additive on long-range scales.[41] It has been observed that high shear rates can therefore yield higher discharge capacities for high loading electrodes.[41]

4.1.4. Electrode Drying

In the subsequent electrode drying step, the binder which was previously dissolved in the solvent, precipitates out and deposits onto the surfaces of active material and conductive additive.[13,292] Since the binder is required for mechanical stability and is therefore always part of the conductive network, the conductive network is also often referred to as the carbon binder domain.[13,161,162,285,302–304] Binder is usually electronically and ionically insulating and hence increases interfacial resistances when it deposits on surfaces. The amount of binder should therefore be minimized.

Another problem that frequently occurs during drying, especially of thick electrodes, is the sedimentation of active material due to its higher mass. This effect is particularly pronounced if CB was fully deagglomerated in the previous mixing step.[305] Meanwhile, the binder dissolved in the solvent can migrate to the surface, ultimately leading to a binder-enriched surface and active material-enriched lower part of the electrode.[306] Hence, choosing a sufficiently high drying temperature is crucial to avoid excessive segregation.[41]

4.1.5. Electrode Calendaring

In the final step, electrodes are often calendared to reduce porosity and thereby increase volumetric energy density. Moreover, calendaring improves electronic contacts both within the conductive network and between the active material and conductive network.[81,159,166,307] Calendaring is also important to improve mechanical stability and contact between the electrode and current collector.[307] However, CB is hard to compress during calendaring because of high repulsive forces of the electrical charges

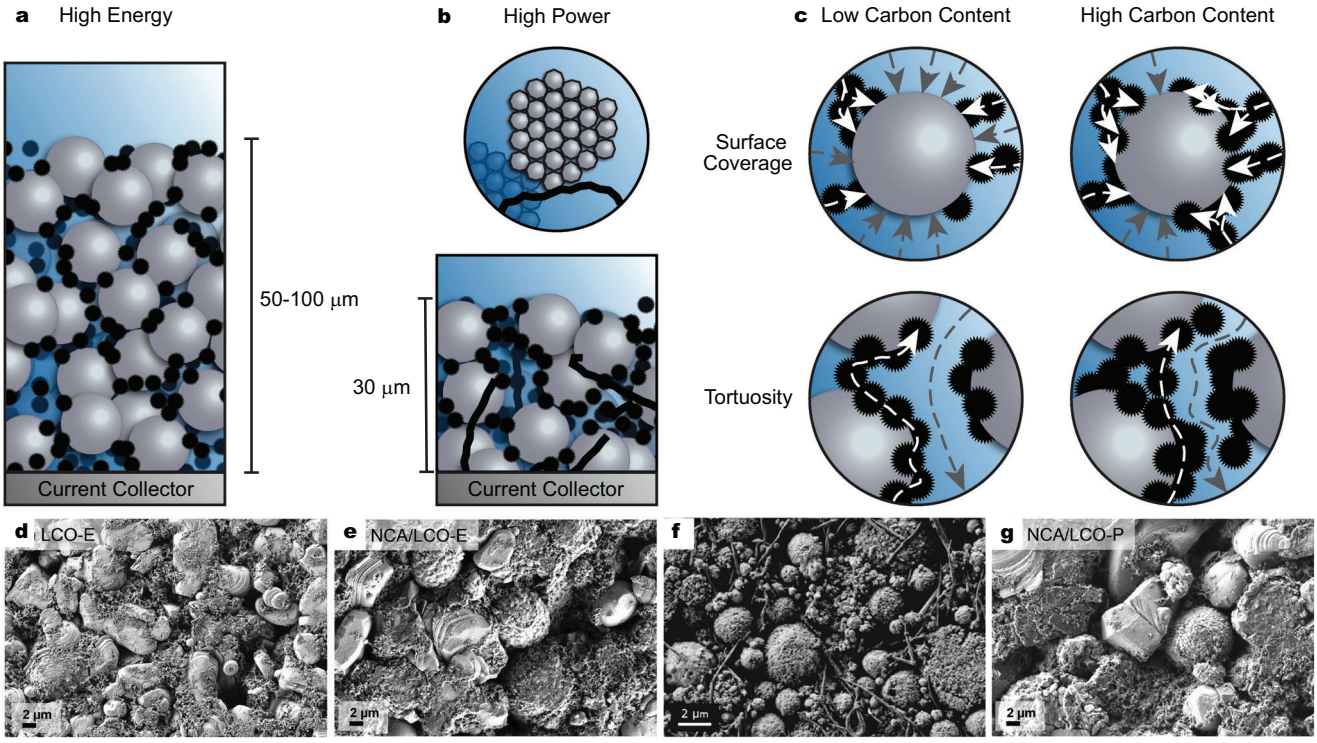

Figure 6. Structure of conductive networks in state-of-the-art electrodes. a,b) Schematic representation of high-energy (a) and high-power (b) electrodes. The schematic for the VGCF highway was adapted with permission.[312]. Copyright 2015, Royal Society of Chemistry. c,d) Influence of carbon content on surface coverage and tortuosity for Li-ion and electronic diffusion pathways. d–g) SEM micrographs of commercial cathodes for high-energy (d, e) and high-power (f, g) applications. Reproduced with permission.[220,221] Copyright 2019, Elsevier. Copyright 2012, IOP Science.

on the CB surface.[308] For the production of dense electrodes, a small amount of graphite can help to reduce spring back effects during calendaring and therefore improve the volumetric energy density further.[57] However, the decreased pore size after calendaring usually results in more tortuous Li-ion diffusion pathways.

4.2. Conductive Networks in High-Energy-Density Electrodes

4.2.1. Structure of Commercialized State-of-the-Art High-Energy Density Electrodes

In this section, we review the structure of commercialized state-of-the-art high-energy-density electrodes. When attempting to improve the energy density of LIBs, a primary consideration is increasing the electrode mass and thickness. This approach increases the proportion of active material relative to inactive cell components, such as current collectors and separators, etc. However, the electrode thickness cannot be increased indefinitely, because mechanical cracking occurs during drying beyond the critical cracking thickness.[309] State-of-the-art electrodes, for instance, are about 50 to 100 µm thick (**Figure 6**a).

To further enhance the energy density of LIBs, reducing the content of non-active materials within the electrode itself becomes essential. This involves minimizing carbon contents (< 2 wt.-%),[13] and void fractions (20 to 30 vol.-%).[220,221] At such low carbon contents, homogeneous carbon distribution and good contact with the active material are paramount to ensure full utilization of the entire active material during cycling, even if it results in suboptimal ionic transport.[284,287]

Achieving electronic percolation at long, medium, and short ranges at low carbon contents is commonly realized through the utilization of CB, owing to its small particle size. For instance, Super C65 and Super P are prevalent choices for LCO and NMC cathodes.[57,162,167,285,307,310,311] However, it is noteworthy that relying solely on CB as a conductive additive leads to a reduction in electrode density and, consequently, the volumetric energy density of LIBs due to the high porosity of CB. To address this, small amounts of denser carbon materials, such as conductive graphite KFS6, may be added in conjunction with CB to increase the volumetric energy density of the electrode.[57,162,167,285,307,310,311] Similar considerations apply when employing carbon coatings. While carbon coatings can indeed ensure high conductivity at medium and short ranges, the carbon content in the form of coating should be maintained below 2 wt.-% to uphold the high density of the electrodes and, accordingly, the high volumetric density of the LIBs.

To elucidate the architecture of the conductive network in commercial high-power and high-energy cathodes, Ivers-Tiffee et al. recently conducted a comprehensive characterization of two commercial cylindrical cells (18 500 Sanyo and 18 650 Sony), and two pouch cells (Kokam) for high-power and high-energy applications (Figure 6c–g).[220] Cathodes in high-energy batteries had slightly higher carbon contents (*ca.* 10 to 20 vol.-%) compared to high-power batteries. As a result, the surface of the active material

in high-energy-density cathodes exhibited a greater fraction of CB coverage in contrast to the high-power electrodes (10% compared to 2%, as depicted in Figure 6c). Concurrently, the utilization of elevated carbon contents led to a 50% increased in the electrode tortuosity and the obstruction of Li-ion transport to/from the surface of the active material (Figure 6c).[220,313]

4.2.2. Emerging Strategies for High-Energy-Density Electrodes

In an effort to improve the energy density of electrodes, electrode thicknesses need to be increased even further.[23–25,309] CNTs emerge as a potential solution to overcome the critical cracking thickness associated with CB-containing electrodes, owing to their exceptionally high mechanical strength.[67,314] Notably, Nicolosi et al. demonstrated that the utilization of CNTs as conductive additives allowed the fabrication of extremely thick electrodes (800 µm) without the need for additional binder.[67] Consequently, very high areal loadings of 45 mAh cm^{-2} for Si anodes and 30 mAh cm^{-2} for NMC cathodes could be achieved at relatively low CNT loadings. A corresponding full cell exhibited a remarkable areal capacity of 29 mAh cm^{-2}, although cycling stability could only be demonstrated for 50 cycles.

While increasing the electrode thickness can result in significantly improved energy densities, critical challenges toward commercializing this approach remain. For instance, the design of ultra-thick electrodes may also require novel electrode fabrication processes, such as 3D printing,[315,316] which are not yet cost-effective. Therefore, further reduction of carbon content below the industry standard of 2 wt.-% may be more practical in the short-term. As discussed in Section 2.3.1, high aspect ratio conductive additives may offer significant advantages in this respect because of their significantly lower percolation thresholds. A plethora of work is therefore investigating these conductive additives in high-energy electrodes, e.g. SWCNTs,[67,169,206,314,317] MWCNT,[155,157,208,318–321] VGCF,[312,320,322] or RGO.[156–158,160,169,243,244,250,255,323–326] For example, the use of RGO allows significantly lower percolation thresholds compared to those observed with commercial conductive additives.[156,157,160,244] Its 2D planar structure can also offer improved conductivity on the short-range scale due to its larger contact area with the active material. However, the planar structure of graphene also causes significantly more tortuous Li-ion pathways, and impedes Li-ion transport to the active material.[160] The applicability of RGO nanosheets for high-energy and high-power LFP-based LIBs was studied by Kang et al.[156,157] Their studies demonstrated higher capacities for RGO-containing electrodes (2 wt.-% carbon) at low C-rates (up to 2 C) compared to a conventional CB-based composition (10 wt.-% carbon). Concomitantly, high overpotentials for the RGO-containing electrodes resulted in a drastic capacity loss at high rates. The authors attributed this behavior to the Li-ion-blocking nature of graphene.[156] Hence, graphene could be appealing for high-energy density, but not high-power density applications.

It is noteworthy that high surface area conductive additives such as CNTs or graphene can present challenges in terms of electrode fabrication. CNTs and graphene tend to agglomerate during slurry preparation due to strong van der Waals interactions between particles.[208] Agglomeration may be prevented by functionalization,[208] or stabilization with surfactants.[67] However, functionalization reduces the electronic conductivity in the conductive network and thus the rate capability, while surfactant needs to be carbonized subsequently under an inert atmosphere. This process usually takes place at around 700 °C, which puts severe constraints on other cell components regarding their thermal stability.

4.3. Conductive Networks in High-Power-Density Electrodes

Commercial high-energy-density batteries contain electrodes with maximized active material contents and are therefore not optimized for high-power applications. The rate capability of commercial high-energy electrodes is mainly limited by poor long-range ionic transport due to the very high electrode thicknesses and highly tortuous Li-ion pathways. To overcome the bottleneck of ionic conductivity, the ionic transport pathways in high-power density electrodes are significantly shorter. This is achieved by i) reducing the electrode thickness (to *ca.* 30 µm) to facilitate Li-ion electrolyte penetration, and ii) lowering the carbon contents (to *ca.* 5 to 15 vol.-%), to reduce the tortuosity of Li-ion diffusion pathways.[220] Since the carbon contents in high-power electrodes can be even lower than in high-energy electrodes, retaining high electronic conductivity requires reducing the percolation threshold. High-power density electrodes may therefore employ a cost-effective high aspect ratio conductive additives like VGCF (Figure 6b).[220,221]

In addition to the use of high aspect ratio carbon additives, other strategies for the fabrication of high-power electrodes are under intense investigation.[23–25] A common theme of most emerging high-power conductive networks is the construction of low tortuosity Li-ion pathways. For instance, magnetically aligned conductive networks can be used to significantly reduce the tortuosity in graphite anodes,[327] or LCO cathodes.[328] Similarly, laser patterning is a viable technique to reduce the tortuosity factor.[329] Alternatively, ordered conductive networks can be constructed by the synthesis of tailored ordered scaffolds, e.g. through co-extrusion/sintering.[330]

With respect to Li-ion diffusion bottlenecks on the short-range scale, Li-ion diffusion to/from the active material may be impeded by carbon coatings. Carbon coatings should therefore be less than 3 nm thick and exhibit significant porosity in the amorphous carbon domains.[272] Simultaneously, the presence of graphitic domains is crucial for electronic conduction. Therefore, the degree of graphitization is critical to the ability of the carbon coating to deliver both electrons and ions effectively to the active material.[331]

4.4. Cycling Stability of the Electrodes

The conductive network plays a crucial role in mediating various side reactions that occur after battery assembly and during its subsequent cycling. These side reactions primarily arise from i) the (electro)chemical instability inherent to the conductive network itself,[139,141] and ii) the significant surface area it provides, which enables various electrochemically induced side reactions involving the Li-ion electrolyte and active material to occur.[141,143]

Regarding the (electro)chemical stability of the conductive network, there is evidence that electrolytes may react chemically with the carbon conductive additive, even in the absence of potential or current.[94] Moreover, the conductive network can react electrochemically, especially at high voltages. For instance, oxygen-containing surface functional groups may be oxidized to form CO and/or CO_2.[140] The electrochemical stability of the conductive network is therefore highly sensitive to the chemical structure of the carbon material itself.[139] For instance, commercial CB like C65 has been optimized for excellent oxidative stability, but side reactions will be much more pronounced in high surface area carbon materials with low degrees of graphitization due to their abundant surface functional groups. Likewise, the chemical composition of the electrolyte, e.g. the solvent,[141] Li-salt,[141] and impurities, such as trace amounts of H_2O,[140,165,332] all determine the electrochemical stability window of the conductive network. For instance, no significant carbon oxidation is observed for Super C65 CB at room temperature in $LiPF_6$/EC electrolytes, even above 5 V.[141] However, C65 oxidation becomes more pronounced at moderate temperatures (50 °C) or can start occurring at voltages as low as 4.5 V, e.g. in $LiClO_4$-containing electrolytes.[141]

When considering electrochemically induced side reactions occurring at the electrode surface, it is crucial to bear in mind that even at moderate carbon contents in the electrode, the conductive network dominates the total electrode surface area. For instance, in a typical electrode, comprised of transition metal oxide active material (90 wt.-%, *ca.* 0.2 to 0.3 $m^2\ g^{-1}$ specific surface area) and C65 CB (5 wt.-%, 65 $m^2\ g^{-1}$ specific surface area), the conductive network accounts for over 90% of the total electrode surface area. Likewise, the electrode surface area will be dominated (>99%) by the contribution of the conductive network, even at very low carbon contents below 1 wt.-%, for carbon materials like CNTs or graphene, with surface areas many orders of magnitude higher than for CB. In the absence of any catalytic activity of either the active material or the conductive networks, electrolyte degradation is therefore dominated by the reactions occurring on the conductive network surface, as discussed by Gasteiger et al.[143] Understanding the chemical and electrochemical stability of different battery components, especially the electrolyte, under operating conditions and in the presence of the conductive networks is therefore crucial.[82,143,144,333,334] It should be noted that electrolyte degradation on the carbon surface is not restricted to high-voltage cathodes. Dahn et al. demonstrated that electrodes containing higher Super S CB contents and therefore a larger surface area exhibited lower coulombic efficiencies than Li/graphite cells containing less CB, when cycled between 0.05 and 1.2 V.[82]

This deteriorating effect of high surface area conductive additives on electrolyte degradation is not very well studied in the literature, and most papers on CNTs or graphene do not demonstrate cycling stabilities beyond 100 cycles at relevant loadings.[155,169,206,208,318–321,335] While some reports highlight the cycling stability in the presence of CNTs,[116,336] other reports find somewhat lower coulombic efficiencies and stability in the presence of CNTs relative to CB-containing conductive networks.[337,338] Further work in this area may be needed to resolve this question.

Finally, reactive surface functional groups can also contribute to electrolyte degradation.[139,142] The influence of their abundance on the cycling stability of high-voltage cathodes was studied by Winter et al.[144] Thermally treated CB with a reduced amount of functional groups showed improved cycling stability in Lithium nickel manganese oxide cathodes.

5. Conductive Networks in Electrodes with Novel Active Materials

Active materials can be classified according to their lithiation mechanism into three main categories: intercalation, alloying, and conversion materials (**Figure 7**).[184,339–345] The typical examples of intercalation-type materials are the well-established transition metal oxides (e.g., NMC or LCO) and graphite, which can store Li-ions without significant volume changes (< 10 vol.-%) due to the limited number of electrons/Li-ions (≤ 1) involved in the redox reactions per transition metal or C_6 center, respectively. The majority of intercalation-type cathode active materials consist of scarce and expensive transition metals, particularly cobalt and nickel. Recognizing the challenges posed by the scarcity and high cost of these metals, current efforts are underway to develop Co- and Ni-free intercalation-type counterparts. Specifically, research is focused on alternative cathodes such as LMO,[180,346,347] LMP,[154,348,349] and LVP.[350] Additionally, investigations are ongoing for high-capacity materials derived from known active materials, such as Ni-rich NMC,[351,352] as well as Li-excess materials with layered structures,[353–355] or disordered rock-salt (DRX) structure.[356,357] Similarly, other transition metal salts are heavily investigated, e.g. V_2O_5,[209,358,359] or iron fluorides with pyrochlore,[337,360] or hexa-tungsten bronze structure.[361]

Moving onto alloying-type materials, the primary rationale for employing them as active materials stems from their substantial charge-storage capacity, which is attributed to the involvement of multiple electrons per redox center (Figure 7b).[362] Prominent examples in this category include Si,[113,363–367] Sn,[12,368–373] and Sb.[12,372,374] For the purposes of this review, metallic Li can be considered as an alloying-type active material, and conductive networks to utilize metallic Li have been heavily investigated as well.[114,375,376] Despite their high charge-storage capacities of over 4000 mAh g^{-1} for Si, due to the reversible acceptance/release of up to 4.4 electrons per active material,[363] lithiation of alloying-type anodes leads to their severe volume changes of several hundred percent,[377,378] which poses significant challenges to their cycling stability.[379]

Similarly, conversion-type materials also exhibit very high capacities due to the involvement of multiple electrons per redox center. Lithiation causes the formation of new phases, thus defining these materials as conversion-type (Figure 7c). Sulfur is a particularly interesting example of a conversion-type cathode material because of its high theoretical capacity of 1675 mAh g^{-1} for two-electron reduction, resulting in the formation of Li_2S.[110,380–385] Simultaneously, sulfur stands out as the active material with the lowest electronic conductivity (10^{-30} S cm^{-1}). Further examples of conversion-type cathodes encompass transition metals such as FeF_x,[8,107,108,361,386–398] CoF_2,[391,399] MnF_2,[391,400] CuF_2,[401] and BiF_3.[402–406] While the discharge potential of these materials is similar to or higher than that of sulfur, their theoretical charge storage capacities are lower, reaching a maximum of 730 mAh g^{-1}. At the same time, their significantly higher electronic and ionic conductivity compared to sulfur make their

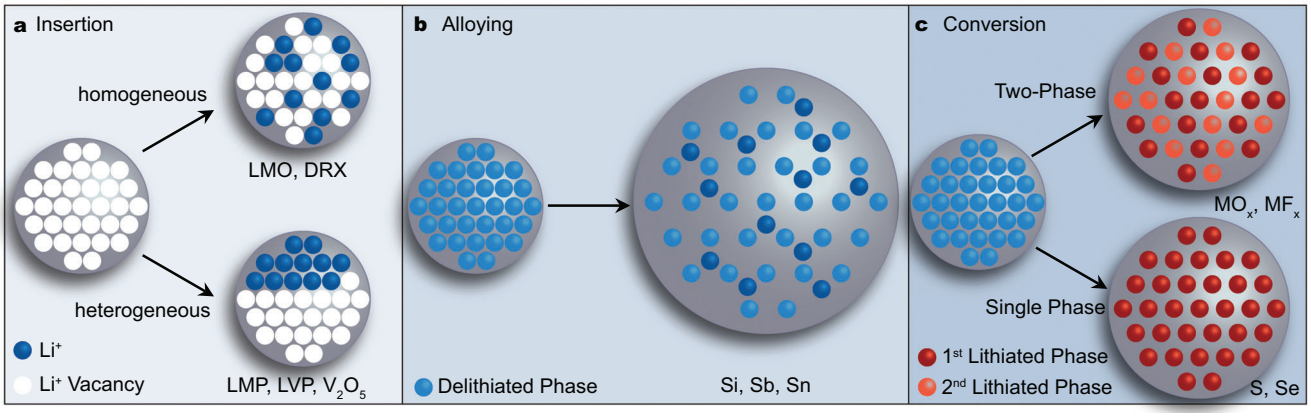

Figure 7. Different lithiation mechanisms of novel active materials. Adapted with permission.[339] Copyright 2009, Royal Society of Chemistry.

applicability potentially more viable. Lastly, transition metal oxides, including CoO_x,[245,407–410] FeO_x,[407,411–416] MnO_x,[115,238,407,417,418] NiO_x,[256,407,419] and TiO_x,[11,420] are currently subject to intensive investigations owing to their potential as compelling conversion-type anodes, characterized by their high theoretical capacities around 1000 mAh g^{-1}, and low discharge potentials (0.5 to 1 vs Li^+/Li).[339,407]

Given the significant variations in electrochemical properties among active materials, the design and fabrication of electrodes for each mentioned category must address distinct and specific challenges tailored to the unique characteristics of the corresponding active material.[184,340–345] Nevertheless, some issues are common across materials from different categories, and a concise summary of these common issues is presented below.

The primary and overarching challenge for all novel active materials with high charge-storage capacity is the occurrence of volume changes during cycling. The expansion in volume results in delamination of active materials from the conducting network, leading to a decreased charge-storage capacity (**Figure 8**a). It is important to note, however, that the degree of volume change varies across different materials. For instance, novel intercalation-type electrodes, or conversion-type BiF_3[402,405,406] exhibit volume changes comparable to, or only slightly exceeding those of commercialized intercalation-type materials. To evaluate

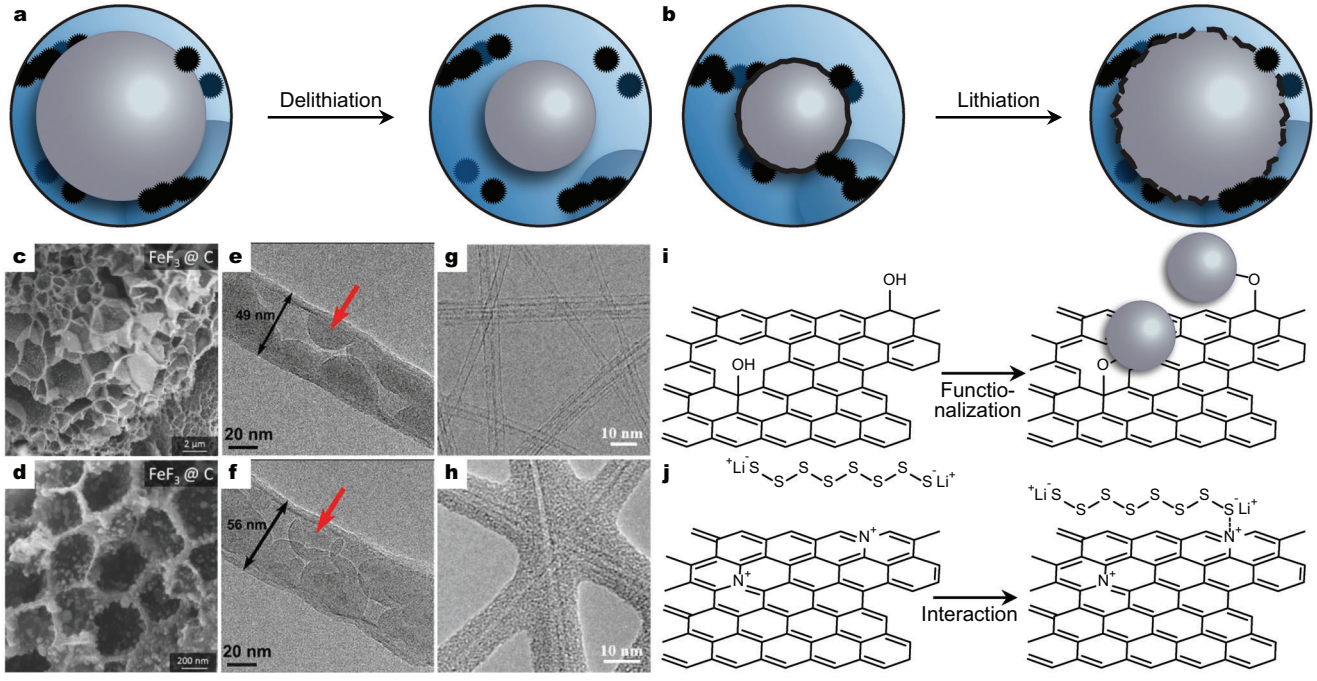

Figure 8. Tailored conductive networks for the study of novel active materials. a,b) Failure of conductive networks based on conventional conductive additives (a) and carbon coatings (b). c,d) FeF_3 nanoparticles on 3D honeycomb structure of carbon. Reprinted with permission.[390] Copyright 2019, Wiley. e,f) Silicon nanoparticles contained within SWCNTs before (e) and after (f) cycling. Reprinted with permission.[197] Copyright 2015, Royal Society of Chemistry. g,h) CNT wireframe before (g) and after (h) sulfur impregnation. Reprinted with permission.[421] Copyright 2017, Elsevier. i,j) Immobilization strategies based on the anchoring of active material (Adapted with permission.[230] Copyright 2015, Nature.) (i) or reactants (j).

the intrinsic electrochemical performance of novel active materials with such relatively small volume changes, a straightforward approach involves adopting similar fabrication processes to those discussed in Section 4. However, materials exhibiting substantial volume changes require alternative approaches, which will be discussed in the following section.

A second notable concern of many novel active materials is the low electronic conductivity of the active material. This implies that high resistances within the active material (R_{AM}) can dominate the total resistance according to Equation 1 unless the diffusion length (l_{AM}) is minimized. While the apparent solution to this problem is nanostructuring,[182,347,350,358,422,423] achieving close contact between the nanostructured active material and the conductive network is a challenging task. A straightforward strategy for addressing the issue of low electronic conductivity in active materials involves employing a premixing step via high-energy ball milling of the active material with carbon additives. This step can help reduce interfacial resistance and control the active material particle size.[402,424] Carbon contents in this case, can vary between 5 to 20 wt.-%, although values as high as 40 wt.-% are reported.[107,337,358,380,390,402] Moreover, the addition of CNTs or graphene to the electrode can enhance the electronic contact between the conductive network and the active material due to the higher interfacial contact area (A_{int}).[155,209,246,337,359,402,425,426] Lastly, carbon coatings can also be considered a viable solution to this problem, but it is important to note that this approach is effective primarily for active materials with small volume changes, as carbon coatings possess low mechanical stability and may crack in response to significant volume changes (Figure 8b).[427]

Finally, there are some issues related to the loss of structural integrity of the electrode, which can be the result of leaching of active material. The most typical example of this problem is the dissolution of polysulfides in organic electrolytes formed during the discharge of Li-S batteries.[110,184]

5.1. Tailored Conductive Networks

In the preceding discussion, we briefly outlined the most critical challenges associated with incorporating novel active materials into LIBs, along with some initial strategies to address them. It is important to note that these strategies are suitable for the preliminary screening of novel active materials, and more sophisticated approaches are essential, particularly when dealing with significant volume expansion during lithiation/delithiation and poor electronic conductivity of the active material.

In this context, the use of porous carbon scaffolds emerges as a potential solution to tackle the issues of volume changes and electronic conductivity. Carbon scaffolds refer to carbon materials with finely distributed interconnected pores. Infiltrating these pores with active material can reduce the diffusion pathways within the poorly conductive active material (l_{AM}). Examples of carbon scaffolds include various forms of mesoporous carbon and carbon monoliths. For more detailed reviews on carbon scaffolds, the reader is referred elsewhere.[428–436]

Mesoporous carbon consists of micron-sized particles characterized by pore sizes ranging from 2 to 50 nm. The advantages of porous scaffolds were initially showcased in Li-S batteries by Nazar et al.[380] The infiltration of sulfur melt into CMK-3 mesoporous carbon proved highly effective, leading to an exceptional increase in capacity compared to a conventional cathode design that utilized acetylene black as the conductive additive.

A carbon monolith is a microscopic, free-standing porous carbon electrode characterized by high degrees of graphitization, porosity exceeding 90 vol.-%, and a surface area between 100 to 1000 $m^2\ g^{-1}$ (Figure 8c,d). The pore sizes in these materials can vary widely, reaching up to millimeters depending on the synthesis. However, scaffolds employed in electrodes typically exhibit pore sizes of 0.1 to 10 µm with a narrow distribution.[437–439] An example of a carbon monolith is 3D graphene, consisting of 10 or fewer graphene layers.[428] The pore microstructure of 3D graphene and its derivatives can vary widely, with structures such as crumpled, honeycomb, coral, and flower-like reported. Synthesis methods for 3D graphene involve various approaches, including those based on random stacking of RGO sheets,[261,437] templated synthesis,[440,441] CVD growth,[442] and thermal decomposition of polymers.[390] Carbon monoliths, such as 3D graphene, have been widely employed with various active materials, including S,[261,443] Fe_3O_4,[438], FeF_3,[390] and MoS_2.[439,444] Due to the discrete micron-sized domains of its porous structure, additional conductive additives are usually included during electrode preparation to ensure connectivity between the porous segments.[390]

Another strategy for addressing issues related to significant volume changes and low electronic conductivity of active materials involves carbon materials with a high aspect ratio, primarily SWCNTs or CFs. This strategy involves constructing a wireframe network that is infused with active material through either melt infiltration or in situ synthesis of the active material,[365] ensuring close contact and minimizing Li-ions diffusion pathways (Figure 8g,h). Initially applied to Si anodes,[365] this strategy has been extended to various anode and cathode materials, such as Fe_2O_3,[414,445] Co_3O_4,[9] or MoS_2.[7,446] These networks can be highly mechanically stable, permitting their usage as electrodes without additional conductive additives.[365,398,421]

Moreover, non-filling carbon coatings have been developed for active materials that undergo large volume change during cycling.[113,367,427,447] Unlike regular carbon coatings, these coatings trade some of the high contact area with the active material for the ability to accommodate volume change of the active material. Similarly, active materials can be confined in hollow carbon,[371,384,448] in graphene scrolls,[449] in CNTs,[194,195,197,198] or in CNFs[196,450–452] (Figure 8e,f). However, it is important to note that this strategy can only work for porous carbon materials. Otherwise, Li-ion diffusion toward the active material may be hindered, resulting in poor rate capability.

To conclude this section, a few pitfalls for the strategies discussed above need to be kept in mind. Very high porosity, frequently surpassing 90 vol.-%, of these conductive network is a prevailing feature among all the approaches. Hence, the volumetric energy and power density is substantially reduced. Additionally, these conductive networks often display poor mechanical stability, primarily attributed to the fragility of the carbon walls within the structure. Notably, these networks are optimized for conductivity on short- and medium-range scales, while their conductivity on long-range scales may be suboptimal

because of the relatively low carbon contents of the conductive networks. Although not extensively addressed in the literature, it is noteworthy that the majority of papers in this field still resort to incorporating additional carbon additives, such as CB, to establish a more effective conductive network on long-range scales.

5.2. Reactant Immobilization

As elaborated in Section 3, the surface chemistry of conductive carbon materials can be altered to introduce or eliminate functional groups and heteroatoms. While conventional conductive networks benefit from minimizing surface functional groups to maximize electronic conductivity, surface functional groups can play a vital role in facilitating intimate contact between the conductive network and the conversion- or alloying-type active materials. For example, nanoparticulate active material can be grafted onto graphene if reactive functional groups are present on the surface (Figure 8i).[256,418,453] This approach ensures close contact with the conductive network, even in scenarios where the active material undergoes phase transformations or significant volume changes. An illustrative example of such an approach is the synthesis of metal oxide anodes on graphene, including CoO_x,[196,245] NiO_x,[196,256,419] FeO_x,[414] and MnO_x,[115,196,418] FeF_3,[393,396,397,454,455] and SnO_2.[239,370,456] Functionalized CNTs have also been employed to graft various nanostructured conversion materials, such as Fe_2O_3,[414] V_2O_5,[209] or FeF_3.[388]

Reactant immobilization is crucial in Li-S batteries as well. During discharge, polysulfides form, which are soluble in the electrolyte and subsequently leach out of the cathode, leading to capacity fade. Simple physical confinement in hollow carbon spheres is often insufficient because the polar polysulfides interact weakly with apolar carbon in the case of unfunctionalized carbon additives.[184] Hence, the polysulfides need to be chemically immobilized within the cathode.[110] Most often, N-doped graphene is used to immobilize the polysulfides via strong dipole-dipole interactions.[258,260] Similarly, amino-functionalized RGO can help to reduce polysulfide shuttling.[457] With the development of novel synthetic techniques, this approach has also been extended to incorporate other functionalities into the conductive network, e.g., single metal atoms.[458,459] These isolated transition metals are highly active redox mediators for the catalytic conversion of polysulfides.

It should be noted that these immobilization strategies predominantly focus on altering the surface chemistry of carbon rather than addressing the overall structure and morphology of the conductive network. While they can be employed in conjunction with the strategies discussed in Section 5.1, it is crucial to recognize that this approach often leads to a significant reduction in electronic conductivity, and therefore, additional conductive additives are commonly introduced to ensure the required electronic conductivity on long-range scales.

6. Guidelines for the Construction of Electrodes with Effective Conductive Networks

At the outset of this review, we posed the question of how to construct an effective conductive network. As we navigated through the various sections, we delved into the theoretical understanding of electronic conduction in electrodes and explored different conductive additives as the fundamental building blocks for constructing conductive networks. Subsequently, we examined diverse industrially viable, as well as emerging strategies employed to prepare conductive networks, providing insights into effective conductive networks, depending on the research scope. To conclude this discussion, our final goal is to provide a framework that can assist researchers aiming to study the electrochemical performance of different active materials, aiding them in the selection of various additives and methods for constructing an effective conductive network. Within this framework, three central questions must be addressed: 1) What is an "effective" conductive network, given the specific project? 2) What should be the structure and properties of the optimal conductive network? 3) How can the optimal conductive network be achieved practically?

Before entering the laboratory, it is imperative to define the scope of the study and specify which aspects of the active material are under investigation. The scope can vary, ranging from the fundamental electrochemistry of a novel active material, to focusing on enhancing the electrochemical performance of state-of-the-art compounds. Additionally, the targeted electrochemical performance must be clearly defined, such as assessment of gravimetric or volumetric energy density, power density, or cycling stability. This step is pivotal because attempting to optimize all these metrics simultaneously may result in suboptimal outcomes due to the inherent tradeoffs of the conductive network, e.g. between electronic and Li-ion conduction in the electrodes.[289]

Once the research scope is defined, the next critical step is determining the theoretically optimal configuration of the conductive network. For instance, if the focus is on the fundamental electrochemistry of the active material, it becomes imperative to eliminate any ionic and electronic bottlenecks that are unrelated to the active material itself. Moreover, it is essential to discern whether the bottleneck occurs on a short-, medium-, or long-range scale. We have highlighted the importance of length scales for electronic conduction in Section 2, but note that analogous considerations are valid for ionic conduction as well. An additional pivotal aspect involves comprehending the extent of structural and volume changes that occur during cycling of the active material, as highlighted in Section 5.

Once the optimal conductive network has been identified, the subsequent step entails its fabrication. In the realm of basic research, the question may arise as to whether conventional strategies discussed in Section 4 are applicable, or whether the synthesis of a custom conductive network may be required, as discussed in Section 5. When looking for methods, it may be helpful to look at the literature on other active materials for commonalities. If the construction of conductive additives via slurry preparation is suitable, the appropriate conductive additive must be selected, an overview of which is given in Section 3. Again, the choice depends heavily on the scope of the study and the identified bottleneck of the electrode. It is also important to consider the combination of several conductive additives, e.g. highways for long-range and carbon coatings for short- and medium-range conduction.

Crucially, adding more carbon may not always be appropriate if it does not address the bottleneck. If ionic conductivity is the bottleneck, more carbon may negatively affect the tortuosity of

the Li-ion pathways, or block Li-ions from the active material surface, thereby reducing rate capability. While this effect may be negligible at low loadings due to the very thin electrodes, it is essential to consider when demonstrating higher loadings. Similarly, higher carbon content inevitably increases the electrode surface area, which can increase side reactions and ultimately degrade cycling stability, even if the active material itself is potentially stable during cycling. Likewise, even if electronic conductivity is identified as a bottleneck that could theoretically be overcome by higher carbon levels, the interplay of binder and carbon must be considered to ensure that higher carbon levels actually result in higher electronic conductivity over the short, medium, and long scales. This is especially important since excessive amounts of carbon additive may absorb binder, which can then no longer provide mechanical stability to the electrode. If this effect is counteracted by the use of larger amounts of binder, it may lead to higher interfacial resistances between particles of the carbon additive, instead of the desired improved conductivity. Lastly, it is important to keep in mind that the carbon additives might possess considerable intrinsic charge-storage capacities themselves.[158,214,460–465] This can lead to an overestimation of the intrinsic charge-storage capacity and rate capability of a given material when normalized by the active material mass. To estimate the effect of this additional capacity, reference electrodes with similar conductive network loadings without active material can be fabricated and characterized, attributing the capacity difference to the active material.

It should also be noted that the electrode fabrication process requires careful attention, particularly regarding processing conditions that can significantly influence the final conductive network, as elaborated in Section 4.1. For example, it is essential to identify the optimal sequence for mixing components, determine the desired level of deagglomeration of the conductive additive, and establish the optimal speed for the mixing and tape-casting process. Moreover, attention to details such as drying and calendaring is crucial and should not be overlooked.

We conclude this section by emphasizing that the accurate documentation of the electrode fabrication procedure is paramount to ensure its reproducibility by other researchers. For instance, crucial details include specifying the type of conductive additives used, their relative fractions and absolute masses, the quantity of solvent in the slurry, and the method of mixing, e.g. ball milling or other techniques. Even seemingly minor details, such as the material of the ball mill jar, its volume, the size and number of balls, and the specific mixing program, should be reported, as they directly influence the resulting conductive network.

7. Conclusion

In a nutshell, we emphasize that a simple theoretical model, which considers various length scales in the battery electrode, is sufficient to develop valuable intuition for the design and fabrication of battery electrodes with effective conductive network. The presented discussion dispels a commonly held misconception that higher carbon contents and more highly conductive carbon in electrodes would always eliminate the electron transport bottleneck. This assertion is inaccurate, as macroscopic conductivity within the electrode is influenced by more than just these two factors. In this context, we also underscore that, due to the diverse use cases of conductive additives at short-, medium-, and long-range length scales, the fabrication of battery electrodes may be based on the complementary use of multiple conductive additives. We also underline that if the bottleneck of the active material is not known a priori, using too much carbon can significantly increase the tortuosity for Li-ions and, consequently, the ionic resistance, or necessitate the use of additional insulating binder. Furthermore, we reiterate that there are many similarities in conductive networks across different active materials, both for cathodes and anodes. Therefore, we encourage readers to draw inspiration from research on active materials beyond their own. Ultimately, the optimal conductive network will depend on a clearly defined research objective, the properties of the active material, and the identified bottleneck.

Acknowledgements

J.F.B. thanks the Fonds der Chemischen Industrie for a Kekulé doctoral fellowship. J.F.B. thanks I. Quarch, H. Zhang, and F. Okur for helpful discussions.

Open access funding provided by Eidgenossische Technische Hochschule Zurich.

Conflict of Interest

The authors declare no conflict of interest.

Author Contributions

J.F.B. conceptualized the project and wrote the manuscript. K.K. conceptualized and supervised the project and wrote the manuscript. M.K. supervised the project and wrote the manuscript.

Keywords

active material, carbon black, carbon nanotubes, conductive network, energy storage, graphene, Li-ion batteries

Received: January 30, 2024
Revised: April 3, 2024
Published online:

[1] V. Etacheri, R. Marom, R. Elazari, G. Salitra, D. Aurbach, *Energy Environ. Sci.* **2011**, *4*, 3243.
[2] X. Zeng, M. Li, D. Abd El-Hady, W. Alshitari, A. S. Al-Bogami, J. Lu, K. Amine, *Adv. Energy Mater.* **2019**, *9*, 1900161.
[3] Y. Liu, Y. Zhu, Y. Cui, *Nat. Energy* **2019**, *4*, 540.
[4] C. D. Quilty, D. Wu, W. Li, D. C. Bock, L. Wang, L. M. Housel, A. Abraham, K. J. Takeuchi, A. C. Marschilok, E. S. Takeuchi, *Chem. Rev.* **2023**, *123*, 1327.
[5] M. Park, X. Zhang, M. Chung, G. B. Less, A. M. Sastry, *J. Power Sources* **2010**, *195*, 7904.
[6] G. Li, J. Sun, W. Hou, S. Jiang, Y. Huang, J. Geng, *Nat. Commun.* **2016**, *7*, 10601.
[7] Y. M. Chen, X. Y. Yu, Z. Li, U. Paik, X. W. Lou, *Sci. Adv.* **2016**, *2*, 1600021.
[8] X. Hua, A. S. Eggeman, E. Castillo-Martínez, R. Robert, H. S. Geddes, Z. Lu, C. J. Pickard, W. Meng, K. M. Wiaderek, N. Pereira, G. G. Amatucci, P. A. Midgley, K. W. Chapman, U. Steiner, A. L. Goodwin, C. P. Grey, *Nat. Mater.* **2021**, *20*, 841.

[9] Y. M. Chen, L. Yu, X. W. Lou, *Angew. Chem., Int. Ed.* **2016**, *55*, 5990.
[10] B. Wang, W. Al Abdulla, D. Wang, X. S. Zhao, *Energy Environ. Sci.* **2015**, *8*, 869.
[11] H. Liu, W. Li, D. Shen, D. Zhao, G. Wang, *J. Am. Chem. Soc.* **2015**, *137*, 13161.
[12] M. He, M. Walter, K. V. Kravchyk, R. Erni, R. Widmer, M. V. Kovalenko, *Nanoscale* **2015**, *7*, 455.
[13] J. Entwistle, R. Ge, K. Pardikar, R. Smith, D. Cumming, *Renewable Sustainable Energy Rev.* **2022**, *166*, 112624.
[14] S. Khodabakhshi, P. F. Fulvio, E. Andreoli, *Carbon* **2020**, *162*, 604.
[15] M. E. Spahr, in *Lithium-Ion Batteries: Science and Technologies* (Eds: M. Yoshio, R. J. Brodd, A. Kozawa), Springer, New York **2009**, p. 5.
[16] W. Yuan, Y. Zhang, L. Cheng, H. Wu, L. Zheng, D. Zhao, *J. Mater. Chem. A* **2016**, *4*, 8932.
[17] Y. Gogotsi, *Nanotubes and Nanofibers*, CRC press, Boca Raton **2006**.
[18] X.-M. Liu, Z. D. Huang, S. W. Oh, B. Zhang, P.-C. Ma, M. M. F. Yuen, J.-K. Kim, *Compos. Sci. Technol.* **2012**, *72*, 121.
[19] R. Kumar, S. Sahoo, E. Joanni, R. K. Singh, W. K. Tan, K. K. Kar, A. Matsuda, *Prog. Energy Combust. Sci.* **2019**, *75*, 100786.
[20] X. Li, L. Zhi, *Chem. Soc. Rev.* **2018**, *47*, 3189.
[21] S. L. Morelly, N. J. Alvarez, M. H. Tang, *J. Power Sources* **2018**, *387*, 49.
[22] P. Zhu, P. R. Slater, E. Kendrick, *Mater. Des.* **2022**, *223*, 111208.
[23] X. Zhang, Z. Ju, Y. Zhu, K. J. Takeuchi, E. S. Takeuchi, A. C. Marschilok, G. Yu, *Adv. Energy Mater.* **2021**, *11*, 2000808.
[24] W. Ji, H. Qu, X. Zhang, D. Zheng, D. Qu, *Small Methods* **2021**, *5*, 2100518.
[25] Y. Kuang, C. Chen, D. Kirsch, L. Hu, *Adv. Energy Mater.* **2019**, *9*, 1901457.
[26] B. Abeles, H. L. Pinch, J. I. Gittleman, *Phys. Rev. Lett.* **1975**, *35*, 247.
[27] P. Sheng, B. Abeles, Y. Arie, *Phys. Rev. Lett.* **1973**, *31*, 44.
[28] P. Sheng, E. K. Sichel, J. I. Gittleman, *Phys. Rev. Lett.* **1978**, *40*, 1197.
[29] R. de Levie, *Electrochim. Acta* **1963**, *8*, 751.
[30] J. Euler, W. Nonnenmacher, *Electrochim. Acta* **1960**, *2*, 268.
[31] J. Jamnik, J. Maier, *Phys. Chem. Chem. Phys.* **2001**, *3*, 1668.
[32] E. Barsoukov, J. R. Macdonald, *Impedance Spectroscopy: Theory, Experiment, and Applications*, Wiley, Hoboken, NJ **2005**.
[33] J. Moškon, M. Gaberšček, *J. Power Sources Adv.* **2021**, *7*, 100047.
[34] Y. Takahashi, N. Kijima, K. Tokiwa, T. Watanabe, J. Akimoto, *J. Phys. Condens. Matter.* **2007**, *19*, 436202.
[35] D. Carlier, M. Ménétrier, C. Delmas, *J. Mater. Chem.* **2001**, *11*, 594.
[36] R. Amin, Y.-M. Chiang, *J. Electrochem. Soc.* **2016**, *163*, A1512.
[37] R. Amin, P. Balaya, J. Maier, *Electrochem. Solid-State Lett.* **2007**, *10*, A13.
[38] J. Marzec, K. Świerczek, J. Przewoźnik, J. Molenda, D. R. Simon, E. M. Kelder, J. Schoonman, *Solid State Ionics* **2002**, *146*, 225.
[39] B. Marinho, M. Ghislandi, E. Tkalya, C. E. Koning, G. de With, *Powder Technol.* **2012**, *221*, 351.
[40] A. N. Mistry, K. Smith, P. P. Mukherjee, *ACS Appl. Mater. Interfaces* **2018**, *10*, 6317.
[41] R. M. Saraka, S. L. Morelly, M. H. Tang, N. J. Alvarez, *ACS Appl. Energy Mater.* **2020**, *3*, 11681.
[42] S. R. Broadbent, J. M. Hammersley, *Math. Proc. Cambridge Philos. Soc.* **1957**, *53*, 629.
[43] S. Kirkpatrick, *Rev. Mod. Phys.* **1973**, *45*, 574.
[44] K.-J. Euler, R. Kirchhof, H. Metzendorf, *J. Power Sources* **1980**, *5*, 255.
[45] P. J. Flory, *J. Am. Chem. Soc.* **1941**, *63*, 3083.
[46] A. A. Saberi, *Phys. Rep.* **2015**, *578*, 1.
[47] D. Adler, L. P. Flora, S. D. Senturia, *Solid State Commun.* **1973**, *12*, 9.
[48] D. A. G. Bruggeman, *Ann. Phys.* **1935**, *416*, 636.
[49] M. Sahini, *Applications of Percolation Theory*, Taylor & Francis, London **2003**.
[50] S. Nakamura, K. Saito, G. S. Kitagawa, *Jpn. J. Appl. Phys.* **1997**, *36*, 5163.
[51] J. K. W. Sandler, J. E. Kirk, I. A. Kinloch, M. S. P. Shaffer, A. H. Windle, *Polymer* **2003**, *44*, 5893.
[52] A. Nogales, G. Broza, Z. Roslaniec, K. Schulte, I. Šics, B. S. Hsiao, A. Sanz, M. C. García-Gutiérrez, D. R. Rueda, C. Domingo, T. A. Ezquerra, *Macromolecules* **2004**, *37*, 7669.
[53] W. Bauhofer, J. Z. Kovacs, *Compos. Sci. Technol.* **2009**, *69*, 1486.
[54] B. Zhang, Y. Yu, Y. Liu, Z.-D. Huang, Y.-B. He, J.-K. Kim, *Nanoscale* **2013**, *5*, 2100.
[55] Y. Liu, X. He, D. Hanlon, A. Harvey, U. Khan, Y. Li, J. N. Coleman, *ACS Nano* **2016**, *10*, 5980.
[56] C. Zhang, S.-H. Park, O. Ronan, A. Harvey, A. Seral-Ascaso, Z. Lin, N. McEvoy, C. S. Boland, N. C. Berner, G. S. Duesberg, P. Rozier, J. N. Coleman, V. Nicolosi, *Small* **2017**, *13*, 1701677.
[57] M. E. Spahr, D. Goers, A. Leone, S. Stallone, E. Grivei, *J. Power Sources* **2011**, *196*, 3404.
[58] Y. H. Chen, C. W. Wang, G. Liu, X. Y. Song, V. S. Battaglia, A. M. Sastry, *J. Electrochem. Soc.* **2007**, *154*, A978.
[59] H. Kondo, H. Sawada, C. Okuda, T. Sasaki, *J. Electrochem. Soc.* **2019**, *166*, A1285.
[60] D. Stauffer, A. Aharony, *Introduction to Percolation Theory*, Taylor & Francis, London **1994**.
[61] C.-W. Nan, *Prog. Mater. Sci.* **1993**, *37*, 1.
[62] I. Jurewicz, P. Worajittiphon, A. A. K. King, P. J. Sellin, J. L. Keddie, A. B. Dalton, *J. Phys. Chem. B* **2011**, *115*, 6395.
[63] R. Zallen, in *The Physics of Amorphous Solids*, (Ed: R. Zallen), John Wiley & Sons, Inc., Hoboken, NJ **1983**.
[64] F. Du, J. E. Fischer, K. I. Winey, *Phys. Rev. B* **2005**, *72*, 121404.
[65] R. Mezzenga, J. Ruokolainen, G. H. Fredrickson, E. J. Kramer, D. Moses, A. J. Heeger, O. Ikkala, *Science* **2003**, *299*, 1872.
[66] D.-X. Yan, H. Pang, B. Li, R. Vajtai, L. Xu, P.-G. Ren, J.-H. Wang, Z.-M. Li, *Adv. Funct. Mater.* **2015**, *25*, 559.
[67] S.-H. Park, P. J. King, R. Tian, C. S. Boland, J. Coelho, C. Zhang, P. McBean, N. McEvoy, M. P. Kremer, D. Daly, J. N. Coleman, V. Nicolosi, *Nat. Energy* **2019**, *4*, 560.
[68] C.-W. Nan, Y. Shen, J. Ma, *Annu. Rev. Mater. Res.* **2010**, *40*, 131.
[69] I. Balberg, N. Binenbaum, N. Wagner, *Phys. Rev. Lett.* **1984**, *52*, 1465.
[70] Z. Ju, X. Zhang, S. T. King, C. D. Quilty, Y. Zhu, K. J. Takeuchi, E. S. Takeuchi, D. C. Bock, L. Wang, A. C. Marschilok, G. Yu, *Appl. Phys. Rev.* **2020**, *7*, 041405.
[71] B. Vigolo, C. Coulon, M. Maugey, C. Zakri, P. Poulin, *Science* **2005**, *309*, 920.
[72] J. Newman, W. Tiedemann, *AIChE J.* **1975**, *21*, 25.
[73] M. Doyle, T. F. Fuller, J. Newman, *J. Electrochem. Soc.* **1993**, *140*, 1526.
[74] M. Doyle, J. Newman, *Electrochim. Acta* **1995**, *40*, 2191.
[75] T. F. Fuller, M. Doyle, J. Newman, *J. Electrochem. Soc.* **1994**, *141*, 1.
[76] T. C. Choy, *Effective Medium Theory: Principles and Applications*, Oxford University Press, Oxford **2015**.
[77] D. H. Jeon, J. H. Nam, C.-J. Kim, *J. Electrochem. Soc.* **2006**, *153*, A406.
[78] P. Costamagna, P. Costa, V. Antonucci, *Electrochim. Acta* **1998**, *43*, 375.
[79] D. Toker, D. Azulay, N. Shimoni, I. Balberg, O. Millo, *Phys. Rev. B* **2003**, *68*, 041403.
[80] I. Balberg, *Carbon* **2002**, *40*, 139.
[81] W. Bauer, D. Nötzel, V. Wenzel, H. Nirschl, *J. Power Sources* **2015**, *288*, 359.
[82] T. Marks, S. Trussler, A. J. Smith, D. Xiong, J. R. Dahn, *J. Electrochem. Soc.* **2011**, *158*, A51.

[83] F. Croce, A. D' Epifanio, J. Hassoun, A. Deptula, T. Olczac, B. Scrosati, *Electrochem. Solid-State Lett.* **2002**, *5*, A47.
[84] T. M. Higgins, S.-H. Park, P. J. King, C. Zhang, N. McEvoy, N. C. Berner, D. Daly, A. Shmeliov, U. Khan, G. Duesberg, V. Nicolosi, J. N. Coleman, *ACS Nano* **2016**, *10*, 3702.
[85] D. Sun, M. Wang, Z. Li, G. Fan, L.-Z. Fan, A. Zhou, *Electrochem. Commun.* **2014**, *47*, 80.
[86] Y. Tian, Y. An, J. Feng, *ACS Appl. Mater. Interfaces* **2019**, *11*, 10004.
[87] Z. Xiao, Z. Li, P. Li, X. Meng, R. Wang, *ACS Nano* **2019**, *13*, 3608.
[88] C. Zhang, W. Zhao, S.-H. Park, T. Guo, S. Deng, A. Seral-Ascaso, M. Si, R. Grissa, S. Barwich, V. Nicolosi, *Adv. Funct. Mater.* **2023**, *33*, 2213860.
[89] Y. Wu, P. Nie, L. Wu, H. Dou, X. Zhang, *Chem. Eng. J.* **2018**, *334*, 932.
[90] M. Zheng, R. Guo, Z. Liu, B. Wang, L. Meng, F. Li, T. Li, Y. Luo, *J. Alloys Compd.* **2018**, *735*, 1262.
[91] Q. Zhao, Q. Zhu, J. Miao, P. Zhang, P. Wan, L. He, B. Xu, *Small* **2019**, *15*, 1904293.
[92] C. Zhang, S.-H. Park, A. Seral-Ascaso, S. Barwich, N. McEvoy, C. S. Boland, J. N. Coleman, Y. Gogotsi, V. Nicolosi, *Nat. Commun.* **2019**, *10*, 849.
[93] S. Ban, K. Malek, C. Huang, Z. Liu, *Carbon* **2011**, *49*, 3362.
[94] R. Younesi, A. S. Christiansen, R. Scipioni, D.-T. Ngo, S. B. Simonsen, K. Edström, J. Hjelm, P. Norby, *J. Electrochem. Soc.* **2015**, *162*, A1289.
[95] J. H. Warner, N. P. Young, A. I. Kirkland, G. A. D. Briggs, *Nat. Mater.* **2011**, *10*, 958.
[96] J. Gerard Lavin, S. Subramoney, R. S. Ruoff, S. Berber, D. Tománek, *Carbon* **2002**, *40*, 1123.
[97] G. G. Tibbetts, M. L. Lake, K. L. Strong, B. P. Rice, *Compos. Sci. Technol.* **2007**, *67*, 1709.
[98] Z. Zhou, C. Lai, L. Zhang, Y. Qian, H. Hou, D. H. Reneker, H. Fong, *Polymer* **2009**, *50*, 2999.
[99] Y. Hernandez, V. Nicolosi, M. Lotya, F. M. Blighe, Z. Sun, S. De, I. T. McGovern, B. Holland, M. Byrne, Y. K. Gun'Ko, J. J. Boland, P. Niraj, G. Duesberg, S. Krishnamurthy, R. Goodhue, J. Hutchison, V. Scardaci, A. C. Ferrari, J. N. Coleman, *Nat. Nanotechnol.* **2008**, *3*, 563.
[100] J. Heremans, *Carbon* **1985**, *23*, 431.
[101] I. L. Spain, K. J. Volin, H. A. Goldberg, I. Kalnin, *J. Phys. Chem. Solids* **1983**, *44*, 839.
[102] O. C. Compton, S. T. Nguyen, *Small* **2010**, *6*, 711.
[103] J. Sánchez-González, A. Macías-García, M. F. Alexandre-Franco, V. Gómez-Serrano, *Carbon* **2005**, *43*, 741.
[104] Z. Liu, J. Y. Lee, H. J. Lindner, *J. Power Sources* **2001**, *97–98*, 361.
[105] S. Mandal, J. M. Amarilla, J. Ibáñez, J. M. Rojo, *J. Electrochem. Soc.* **2001**, *148*, A24.
[106] A. Yamada, Y. Kudo, K.-Y. Liu, *J. Electrochem. Soc.* **2001**, *148*, A747.
[107] F. Badway, F. Cosandey, N. Pereira, G. G. Amatucci, *J. Electrochem. Soc.* **2003**, *150*, A1318.
[108] F. Badway, N. Pereira, F. Cosandey, G. G. Amatucci, *J. Electrochem. Soc.* **2003**, *150*, A1209.
[109] H. C. Shin, W. I. Cho, H. Jang, *Electrochim. Acta* **2006**, *52*, 1472.
[110] L. Ji, M. Rao, H. Zheng, L. Zhang, Y. Li, W. Duan, J. Guo, E. J. Cairns, Y. Zhang, *J. Am. Chem. Soc.* **2011**, *133*, 18522.
[111] Y. Chen, X. Li, K. Park, J. Song, J. Hong, L. Zhou, Y.-W. Mai, H. Huang, J. B. Goodenough, *J. Am. Chem. Soc.* **2013**, *135*, 16280.
[112] C. Luo, Y. Xu, Y. Zhu, Y. Liu, S. Zheng, Y. Liu, A. Langrock, C. Wang, *ACS Nano* **2013**, *7*, 8003.
[113] N. Liu, Z. Lu, J. Zhao, M. T. McDowell, H.-W. Lee, W. Zhao, Y. Cui, *Nat. Nanotechnol.* **2014**, *9*, 187.
[114] D. Lin, Y. Liu, Z. Liang, H.-W. Lee, J. Sun, H. Wang, K. Yan, J. Xie, Y. Cui, *Nat. Nanotechnol.* **2016**, *11*, 626.
[115] Y. Sun, X. Hu, W. Luo, F. Xia, Y. Huang, *Adv. Funct. Mater.* **2013**, *23*, 2436.
[116] X.-L. Wu, Y.-G. Guo, J. Su, J.-W. Xiong, Y.-L. Zhang, L.-J. Wan, *Adv. Energy Mater.* **2013**, *3*, 1155.
[117] M.-J. Wang, C. A. Gray, S. A. Reznek, K. Mahmud, Y. Kutsovsky, in *Kirk-Othmer Encyclopedia of Chemical Technology*, John Wiley and Sons, Hoboken, NJ **2003**.
[118] C. M. Long, M. A. Nascarella, P. A. Valberg, *Environ. Pollut.* **2013**, *181*, 271.
[119] J.-B. Donnet, *Carbon Black: Science and Technology*, Routledge, New York **1993**.
[120] A. Bianco, H.-M. Cheng, T. Enoki, Y. Gogotsi, R. H. Hurt, N. Koratkar, T. Kyotani, M. Monthioux, C. R. Park, J. M. D. Tarascon, J. Zhang, *Carbon* **2013**, *65*, 1.
[121] Y. Gogotsi, V. Presser, *Carbon Nanomaterials*, CRC Press, Boca Raton **2013**.
[122] P. M. Wilson, F. Orange, M. J. F. Guinel, M. Shekhirev, Y. Gao, J. A. Colon Santana, A. A. Gusev, P. A. Dowben, Y. Lu, A. Sinitskii, *RSC Adv.* **2015**, *5*, 92539.
[123] J. P. Abrahamson, M. Singh, J. P. Mathews, R. L. Vander Wal, *Carbon* **2017**, *124*, 380.
[124] R. Schueler, J. Petermann, K. Schulte, H.-P. Wentzel, *J. Appl. Polym. Sci.* **1997**, *63*, 1741.
[125] B. Partoens, F. M. Peeters, *Phys. Rev. B* **2006**, *74*, 075404.
[126] D. Pantea, H. Darmstadt, S. Kaliaguine, C. Roy, *Appl. Surf. Sci.* **2003**, *217*, 181.
[127] G. Kucinskis, G. Bajars, J. Kleperis, *J. Power Sources* **2013**, *240*, 66.
[128] D. Pantea, H. Darmstadt, S. Kaliaguine, L. Sümmchen, C. Roy, *Carbon* **2001**, *39*, 1147.
[129] H.-J. Choi, M. S. Kim, D. Ahn, S. Y. Yeo, S. Lee, *Sci. Rep.* **2019**, *9*, 6338.
[130] F. Ullmann, W. Foerst, *Encyklopädie der technischen Chemie*, Urban & Schwarzenberg, Munich **1957**.
[131] K. Ono, A. Watanabe, K. Dewa, Y. Matsukawa, Y. Saito, Y. Matsushita, H. Aoki, O. Fukuda, T. Aoki, T. Yamaguchi, *Chem. Eng. J.* **2014**, *250*, 66.
[132] J. Lahaye, *Carbon* **1992**, *30*, 309.
[133] K. H. Homann, *Combust. Flame* **1967**, *11*, 265.
[134] H. F. Calcote, *Combust. Flame* **1981**, *42*, 215.
[135] X. Bourrat, *Carbon* **1993**, *31*, 287.
[136] H. Marsh, E. A. Heintz, F. Rodríguez-Reinoso, *Introduction to Carbon Technologies*, Universidad de Alicante, Spain **1997**.
[137] P. E. Fanning, M. A. Vannice, *Carbon* **1993**, *31*, 721.
[138] H. P. Boehm, *Carbon* **1994**, *32*, 759.
[139] R. Tang, K. Taguchi, H. Nishihara, T. Ishii, E. Morallón, D. Cazorla-Amorós, T. Asada, N. Kobayashi, Y. Muramatsu, T. Kyotani, *J. Mater. Chem. A* **2019**, *7*, 7480.
[140] S. Ishimoto, Y. Asakawa, M. Shinya, K. Naoi, *J. Electrochem. Soc.* **2009**, *156*, A563.
[141] M. Metzger, P. Walke, S. Solchenbach, G. Salitra, D. Aurbach, H. A. Gasteiger, *J. Electrochem. Soc.* **2020**, *167*, 160522.
[142] K. Nueangnoraj, H. Nishihara, T. Ishii, N. Yamamoto, H. Itoi, R. Berenguer, R. Ruiz-Rosas, D. Cazorla-Amorós, E. Morallón, M. Ito, T. Kyotani, *Energy Storage Mater.* **2015**, *1*, 35.
[143] R. Jung, M. Metzger, F. Maglia, C. Stinner, H. A. Gasteiger, *J. Phys. Chem. Lett.* **2017**, *8*, 4820.
[144] X. Qi, B. Blizanac, A. DuPasquier, A. Lal, P. Niehoff, T. Placke, M. Oljaca, J. Li, M. Winter, *J. Electrochem. Soc.* **2015**, *162*, A339.
[145] J. Yan, T. Wei, B. Shao, F. Ma, Z. Fan, M. Zhang, C. Zheng, Y. Shang, W. Qian, F. Wei, *Carbon* **2010**, *48*, 1731.
[146] C. Portet, G. Yushin, Y. Gogotsi, *Carbon* **2007**, *45*, 2511.
[147] P. Trogadas, T. F. Fuller, P. Strasser, *Carbon* **2014**, *75*, 5.
[148] E. Antolini, *Appl. Catal., B.* **2009**, *88*, 1.
[149] A. L. Dicks, *J. Power Sources* **2006**, *156*, 128.

[150] E. Auer, A. Freund, J. Pietsch, T. Tacke, *Appl. Catal., A* **1998**, *173*, 259.
[151] R. Leary, A. Westwood, *Carbon* **2011**, *49*, 741.
[152] S.-M. Oh, S.-W. Oh, C.-S. Yoon, B. Scrosati, K. Amine, Y.-K. Sun, *Adv. Funct. Mater.* **2010**, *20*, 3260.
[153] J. K. Hong, J. H. Lee, S. M. Oh, *J. Power Sources* **2002**, *111*, 90.
[154] S. K. Martha, B. Markovsky, J. Grinblat, Y. Gofer, O. Haik, E. Zinigrad, D. Aurbach, T. Drezen, D. Wang, G. Deghenghi, I. Exnar, *J. Electrochem. Soc.* **2009**, *156*, A541.
[155] J. H. Park, S.-Y. Lee, J. H. Kim, S. Ahn, J.-S. Park, Y. U. Jeong, *J. Solid State Electrochem.* **2010**, *14*, 593.
[156] F.-Y. Su, Y.-B. He, B. Li, X.-C. Chen, C.-H. You, W. Wei, W. Lv, Q.-H. Yang, F. Kang, *Nano Energy* **2012**, *1*, 429.
[157] F.-Y. Su, C. You, Y.-B. He, W. Lv, W. Cui, F. Jin, B. Li, Q.-H. Yang, F. Kang, *J. Mater. Chem.* **2010**, *20*, 9644.
[158] B. L-H Hu, F.-Y. Wu, C.-T. Lin, A. N. Khlobystov, L.-J. Li, *Nat. Commun.* **2013**, *4*, 1687.
[159] H. Bockholt, W. Haselrieder, A. Kwade, *Powder Technol.* **2016**, *297*, 266.
[160] R. Tang, Q. Yun, W. Lv, Y.-B. He, C. You, F. Su, L. Ke, B. Li, F. Kang, Q.-H. Yang, *Carbon* **2016**, *103*, 356.
[161] S. Hein, T. Danner, D. Westhoff, B. Prifling, R. Scurtu, L. Kremer, A. Hoffmann, A. Hilger, M. Osenberg, I. Manke, M. Wohlfahrt-Mehrens, V. Schmidt, A. Latz, *J. Electrochem. Soc.* **2020**, *167*, 013546.
[162] L. S. Kremer, A. Hoffmann, T. Danner, S. Hein, B. Prifling, D. Westhoff, C. Dreer, A. Latz, V. Schmidt, M. Wohlfahrt-Mehrens, *Energy Technol.* **2020**, *8*, 1900167.
[163] J. K. Mayer, H. Bockholt, A. Kwade, *J. Power Sources* **2022**, *529*, 231259.
[164] N. H. Kwon, *Solid State Sci.* **2013**, *21*, 59.
[165] M. Metzger, C. Marino, J. Sicklinger, D. Haering, H. A. Gasteiger, *J. Electrochem. Soc.* **2015**, *162*, A1123.
[166] H. Bockholt, M. Indrikova, A. Netz, F. Golks, A. Kwade, *J. Power Sources* **2016**, *325*, 140.
[167] J. K. Mayer, L. Almar, E. Asylbekov, W. Haselrieder, A. Kwade, A. Weber, H. Nirschl, *Energy Technol.* **2020**, *8*, 1900161.
[168] C. Meyer, M. Weyhe, W. Haselrieder, A. Kwade, *Energy Technol.* **2020**, *8*, 1900175.
[169] R. Tian, N. Alcala, S. J. K. O'Neill, D. V. Horvath, J. Coelho, A. J. Griffin, Y. Zhang, V. Nicolosi, C. O'Dwyer, J. N. Coleman, *ACS Appl. Energy Mater.* **2020**, *3*, 2966.
[170] M. Wang, D. Dang, A. Meyer, R. Arsenault, Y.-T. Cheng, *J. Electrochem. Soc.* **2020**, *167*, 100518.
[171] G.-W. Lee, J. H. Ryu, W. Han, K. H. Ahn, S. M. Oh, *J. Power Sources* **2010**, *195*, 6049.
[172] Z. Bakenov, I. Taniguchi, *J. Power Sources* **2010**, *195*, 7445.
[173] B. L. Cushing, J. B. Goodenough, *Solid State Sci.* **2002**, *4*, 1487.
[174] G. Liu, H. Zheng, A. S. Simens, A. M. Minor, X. Song, V. S. Battaglia, *J. Electrochem. Soc.* **2007**, *154*, A1129.
[175] G. Liu, H. Zheng, S. Kim, Y. Deng, A. M. Minor, X. Song, V. S. Battaglia, *J. Electrochem. Soc.* **2008**, *155*, A887.
[176] G. Liu, H. Zheng, X. Song, V. S. Battaglia, *J. Electrochem. Soc.* **2012**, *159*, A214.
[177] H. Zheng, R. Yang, G. Liu, X. Song, V. S. Battaglia, *J. Phys. Chem. C* **2012**, *116*, 4875.
[178] H. Hamed, S. Yari, J. D'Haen, F. U. Renner, N. Reddy, A. Hardy, M. Safari, *Adv. Energy Mater.* **2020**, *10*, 2002492.
[179] H. Huang, S. C. Yin, L. F. Nazar, *Electrochem. Solid-State Lett.* **2001**, *4*, A170.
[180] F. Jiao, J. Bao, A. H. Hill, P. G. Bruce, *Angew. Chem., Int. Ed.* **2008**, *47*, 9711.
[181] S. Kuroda, N. Tobori, M. Sakuraba, Y. Sato, *J. Power Sources* **2003**, *119–121*, 924.
[182] J. Yang, J. J. Xu, *J. Electrochem. Soc.* **2006**, *153*, A716.
[183] N. H. Kwon, H. Yin, P. Brodard, C. Sugnaux, K. M. Fromm, *Electrochim. Acta* **2014**, *134*, 215.
[184] R. Fang, K. Chen, L. Yin, Z. Sun, F. Li, H.-M. Cheng, *Adv. Mater.* **2019**, *31*, 1800863.
[185] B. J. Landi, M. J. Ganter, C. D. Cress, R. A. DiLeo, R. P. Raffaelle, *Energy Environ. Sci.* **2009**, *2*, 638.
[186] M. Endo, Y. A. Kim, T. Hayashi, K. Nishimura, T. Matusita, K. Miyashita, M. S. Dresselhaus, *Carbon* **2001**, *39*, 1287.
[187] L. Zhang, A. Aboagye, A. Kelkar, C. Lai, H. Fong, *J. Mater. Sci.* **2014**, *49*, 463.
[188] S. Iijima, *Nature* **1991**, *354*, 56.
[189] C. de las Casas, W. Li, *J. Power Sources* **2012**, *208*, 74.
[190] Q. Zhang, J.-Q. Huang, W.-Z. Qian, Y.-Y. Zhang, F. Wei, *Small* **2013**, *9*, 1237.
[191] L. Wen, F. Li, H.-M. Cheng, *Adv. Mater.* **2016**, *28*, 4306.
[192] Z. W. Pan, S. S. Xie, B. H. Chang, C. Y. Wang, L. Lu, W. Liu, W. Y. Zhou, W. Z. Li, L. X. Qian, *Nature* **1998**, *394*, 631.
[193] K. I. Winey, R. A. Vaia, *MRS Bull.* **2007**, *32*, 314.
[194] F. Jin, S. Xiao, L. Lu, Y. Wang, *Nano Lett.* **2016**, *16*, 440.
[195] D. Kong, X. Li, Y. Zhang, X. Hai, B. Wang, X. Qiu, Q. Song, Q.-H. Yang, L. Zhi, *Energy Environ. Sci.* **2016**, *9*, 906.
[196] H. Tabassum, R. Zou, A. Mahmood, Z. Liang, Q. Wang, H. Zhang, S. Gao, C. Qu, W. Guo, S. Guo, *Adv. Mater.* **2018**, *30*, 1705441.
[197] W.-J. Yu, C. Liu, P.-X. Hou, L. Zhang, X.-Y. Shan, F. Li, H.-M. Cheng, *ACS Nano* **2015**, *9*, 5063.
[198] J. Zhou, D. Zhang, X. Zhang, H. Song, X. Chen, *ACS Appl. Mater. Interfaces* **2014**, *6*, 21223.
[199] C. Journet, W. K. Maser, P. Bernier, A. Loiseau, M. L. de la Chapelle, S. Lefrant, P. Deniard, R. Lee, J. E. Fischer, *Nature* **1997**, *388*, 756.
[200] T. W. Ebbesen, P. M. Ajayan, *Nature* **1992**, *358*, 220.
[201] D. S. Bethune, C. H. Kiang, M. S. de Vries, G. Gorman, R. Savoy, J. Vazquez, R. Beyers, *Nature* **1993**, *363*, 605.
[202] T. Guo, P. Nikolaev, A. Thess, D. T. Colbert, R. E. Smalley, *Chem. Phys. Lett.* **1995**, *243*, 49.
[203] K. Hata, D. N. Futaba, K. Mizuno, T. Namai, M. Yumura, S. Iijima, *Science* **2004**, *306*, 1362.
[204] G. Hu, C. Zhao, S. Zhang, M. Yang, Z. Wang, *Polymer* **2006**, *47*, 480.
[205] Z. Spitalsky, D. Tasis, K. Papagelis, C. Galiotis, *Prog. Polym. Sci.* **2010**, *35*, 357.
[206] M. J. Ganter, R. A. DiLeo, C. M. Schauerman, R. E. Rogers, R. P. Raffaelle, B. J. Landi, *Electrochim. Acta* **2011**, *56*, 7272.
[207] J. Li, P. C. Ma, W. S. Chow, C. K. To, B. Z. Tang, J.-K. Kim, *Adv. Funct. Mater.* **2007**, *17*, 3207.
[208] A. Varzi, C. Täubert, M. Wohlfahrt-Mehrens, *Electrochim. Acta* **2012**, *78*, 17.
[209] M. Sathiya, A. S. Prakash, K. Ramesha, J. M. Tarascon, A. K. Shukla, *J. Am. Chem. Soc.* **2011**, *133*, 16291.
[210] C. Tang, Q. Zhang, M.-Q. Zhao, J.-Q. Huang, X.-B. Cheng, G.-L. Tian, H.-J. Peng, F. Wei, *Adv. Mater.* **2014**, *26*, 6100.
[211] R. Rao, C. L. Pint, A. E. Islam, R. S. Weatherup, S. Hofmann, E. R. Meshot, F. Wu, C. Zhou, N. Dee, P. B. Amama, J. Carpena-Nuñez, W. Shi, D. L. Plata, E. S. Penev, B. I. Yakobson, P. B. Balbuena, C. Bichara, D. N. Futaba, S. Noda, H. Shin, K. S. Kim, B. Simard, F. Mirri, M. Pasquali, F. Fornasiero, E. I. Kauppinen, M. Arnold, B. A. Cola, P. Nikolaev, S. Arepalli, et al., *ACS Nano* **2018**, *12*, 11756.
[212] K. Balasubramanian, M. Burghard, *Small* **2005**, *1*, 180.
[213] A. Hirsch, *Angew. Chem., Int. Ed.* **2002**, *41*, 1853.
[214] S. W. Lee, N. Yabuuchi, B. M. Gallant, S. Chen, B.-S. Kim, P. T. Hammond, Y. Shao-Horn, *Nat. Nanotechnol.* **2010**, *5*, 531.
[215] J.-W. Jung, C.-L. Lee, S. Yu, I.-D. Kim, *J. Mater. Chem. A* **2016**, *4*, 703.
[216] B. Zhang, F. Kang, J.-M. Tarascon, J.-K. Kim, *Prog. Mater. Sci.* **2016**, *76*, 319.

[217] M. Inagaki, Y. Yang, F. Kang, *Adv. Mater.* **2012**, *24*, 2547.
[218] T. Koyama, M. Endo, *Jpn. J. Appl. Phys.* **1974**, *13*, 1175.
[219] M. H. Al-Saleh, U. Sundararaj, *Carbon* **2009**, *47*, 2.
[220] L. Almar, J. Joos, A. Weber, E. Ivers-Tiffée, *J. Power Sources* **2019**, *427*, 1.
[221] M. Ender, J. Joos, T. Carraro, E. Ivers-Tiffée, *J. Electrochem. Soc.* **2012**, *159*, A972.
[222] A. K. Geim, K. S. Novoselov, *Nat. Mater.* **2007**, *6*, 183.
[223] A. K. Geim, *Science* **2009**, *324*, 1530.
[224] S. Park, R. S. Ruoff, *Nat. Nanotechnol.* **2009**, *4*, 217.
[225] D. R. Dreyer, S. Park, C. W. Bielawski, R. S. Ruoff, *Chem. Soc. Rev.* **2010**, *39*, 228.
[226] K. S. Novoselov, A. K. Geim, S. V. Morozov, D. Jiang, Y. Zhang, S. V. Dubonos, I. V. Grigorieva, A. A. Firsov, *Science* **2004**, *306*, 666.
[227] M. D. Stoller, S. Park, Y. Zhu, J. An, R. S. Ruoff, *Nano Lett.* **2008**, *8*, 3498.
[228] W. Lv, Z. Li, Y. Deng, Q.-H. Yang, F. Kang, *Energy Storage Mater.* **2016**, *2*, 107.
[229] M. F. El-Kady, Y. Shao, R. B. Kaner, *Nat. Rev. Mater.* **2016**, *1*, 16033.
[230] R. Raccichini, A. Varzi, S. Passerini, B. Scrosati, *Nat. Mater.* **2015**, *14*, 271.
[231] K. Chen, S. Song, F. Liu, D. Xue, *Chem. Soc. Rev.* **2015**, *44*, 6230.
[232] H. Pang, T. Chen, G. Zhang, B. Zeng, Z.-M. Li, *Mater. Lett.* **2010**, *64*, 2226.
[233] D. Wang, X. Zhang, J.-W. Zha, J. Zhao, Z.-M. Dang, G.-H. Hu, *Polymer* **2013**, *54*, 1916.
[234] Z.-S. Wu, G. Zhou, L.-C. Yin, W. Ren, F. Li, H.-M. Cheng, *Nano Energy* **2012**, *1*, 107.
[235] M. Khan, M. N. Tahir, S. F. Adil, H. U. Khan, M. R. H. Siddiqui, A. A. Al-warthan, W. Tremel, *J. Mater. Chem. A* **2015**, *3*, 18753.
[236] D. A. Dikin, S. Stankovich, E. J. Zimney, R. D. Piner, G. H. B. Dommett, G. Evmenenko, S. T. Nguyen, R. S. Ruoff, *Nature* **2007**, *448*, 457.
[237] O. Chuhei, N. Ayato, *J. Phys.: Condens. Matter.* **1997**, *9*, 1.
[238] L. Li, A.-R. O. Raji, J. M. Tour, *Adv. Mater.* **2013**, *25*, 6298.
[239] J. Lin, Z. Peng, C. Xiang, G. Ruan, Z. Yan, D. Natelson, J. M. Tour, *ACS Nano* **2013**, *7*, 6001.
[240] S. Stankovich, D. A. Dikin, R. D. Piner, K. A. Kohlhaas, A. Kleinhammes, Y. Jia, Y. Wu, S. T. Nguyen, R. S. Ruoff, *Carbon* **2007**, *45*, 1558.
[241] D. Li, M. B. Müller, S. Gilje, R. B. Kaner, G. G. Wallace, *Nat. Nanotechnol.* **2008**, *3*, 101.
[242] W. Lv, D.-M. Tang, Y.-B. He, C.-H. You, Z.-Q. Shi, X.-C. Chen, C.-M. Chen, P.-X. Hou, C. Liu, Q.-H. Yang, *ACS Nano* **2009**, *3*, 3730.
[243] Y. Ding, Y. Jiang, F. Xu, J. Yin, H. Ren, Q. Zhuo, Z. Long, P. Zhang, *Electrochem. Commun.* **2010**, *12*, 10.
[244] C. Venkateswara Rao, A. Leela Mohana Reddy, Y. Ishikawa, P. M. Ajayan, *ACS Appl. Mater. Interfaces* **2011**, *3*, 2966.
[245] X.-L. Huang, R.-Z. Wang, D. Xu, Z.-L. Wang, H.-G. Wang, J.-J. Xu, Z. Wu, Q.-C. Liu, Y. Zhang, X.-B. Zhang, *Adv. Funct. Mater.* **2013**, *23*, 4345.
[246] R. Jiang, C. Cui, H. Ma, *Phys. Chem. Chem. Phys.* **2013**, *15*, 6406.
[247] W. S. Hummers Jr., R. E. Offeman, *J. Am. Chem. Soc.* **1958**, *80*, 1339.
[248] N. I. Kovtyukhova, P. J. Ollivier, B. R. Martin, T. E. Mallouk, S. A. Chizhik, E. V. Buzaneva, A. D. Gorchinskiy, *Chem. Mater.* **1999**, *11*, 771.
[249] M. Hirata, T. Gotou, S. Horiuchi, M. Fujiwara, M. Ohba, *Carbon* **2004**, *42*, 2929.
[250] X. Zhou, F. Wang, Y. Zhu, Z. Liu, *J. Mater. Chem.* **2011**, *21*, 3353.
[251] V. Georgakilas, M. Otyepka, A. B. Bourlinos, V. Chandra, N. Kim, K. C. Kemp, P. Hobza, R. Zboril, K. S. Kim, *Chem. Rev.* **2012**, *112*, 6156.
[252] W. Yu, L. Sisi, Y. Haiyan, L. Jie, *RSC Adv.* **2020**, *10*, 15328.
[253] V. D. Punetha, S. Rana, H. J. Yoo, A. Chaurasia, J. T. McLeskey, M. S. Ramasamy, N. G. Sahoo, J. W. Cho, *Prog. Polym. Sci.* **2017**, *67*, 1.
[254] W. J. Lee, U. N. Maiti, J. M. Lee, J. Lim, T. H. Han, S. O. Kim, *Chem. Commun.* **2014**, *50*, 6818.
[255] J. Ha, S.-K. Park, S.-H. Yu, A. Jin, B. Jang, S. Bong, I. Kim, Y.-E. Sung, Y. Piao, *Nanoscale* **2013**, *5*, 8647.
[256] G. Zhou, D.-W. Wang, L.-C. Yin, N. Li, F. Li, H.-M. Cheng, *ACS Nano* **2012**, *6*, 3214.
[257] G. Zhou, L.-C. Yin, D.-W. Wang, L. Li, S. Pei, I. R. Gentle, F. Li, H.-M. Cheng, *ACS Nano* **2013**, *7*, 5367.
[258] Y. Qiu, W. Li, W. Zhao, G. Li, Y. Hou, M. Liu, L. Zhou, F. Ye, H. Li, Z. Wei, S. Yang, W. Duan, Y. Ye, J. Guo, Y. Zhang, *Nano Lett.* **2014**, *14*, 4821.
[259] G. Zhou, S. Pei, L. Li, D.-W. Wang, S. Wang, K. Huang, L.-C. Yin, F. Li, H.-M. Cheng, *Adv. Mater.* **2014**, *26*, 625.
[260] G. Zhou, E. Paek, G. S. Hwang, A. Manthiram, *Nat. Commun.* **2015**, *6*, 7760.
[261] G. Hu, C. Xu, Z. Sun, S. Wang, H.-M. Cheng, F. Li, W. Ren, *Adv. Mater.* **2016**, *28*, 1603.
[262] K. M. Kim, W. S. Jeon, I. J. Chung, S. H. Chang, *J. Power Sources* **1999**, *83*, 108.
[263] O. Hassel, H. Mark, *Z. Phys.* **1924**, *25*, 317.
[264] H. S. Lipson, A. R. Stokes, W. L. Bragg, *Proc. R. Soc. A: Math. Phys. Eng. Sci.* **1942**, *181*, 101.
[265] H. O. Pierson, in *Handbook of Carbon, Graphite, Diamonds and Fullerenes* (Ed: H. O. Pierson), William Andrew Publishing, Oxford **1993**.
[266] J. Wang, X. Sun, *Energy Environ. Sci.* **2012**, *5*, 5163.
[267] H. Li, H. Zhou, *Chem. Commun.* **2012**, *48*, 1201.
[268] L.-X. Yuan, Z.-H. Wang, W.-X. Zhang, X.-L. Hu, J.-T. Chen, Y.-H. Huang, J. B. Goodenough, *Energy Environ. Sci.* **2011**, *4*, 269.
[269] M. M. Doeff, Y. Hu, F. McLarnon, R. Kostecki, *Electrochem. Solid-State Lett.* **2003**, *6*, A207.
[270] S. Yang, Y. Song, K. Ngala, P. Y. Zavalij, M. S Whittingham, *J. Power Sources* **2003**, *119–121*, 239.
[271] Y. Hu, M. M. Doeff, R. Kostecki, R. Fiñones, *J. Electrochem. Soc.* **2004**, *151*, A1279.
[272] R. Dominko, M. Bele, M. Gaberšček, M. Remskar, D. Hanzel, S. Pejovnik, J. Jamnik, *J. Electrochem. Soc.* **2005**, *152*, A607.
[273] M. Gaberšček, R. Dominko, J. Jamnik, *Electrochem. Commun.* **2007**, *9*, 2778.
[274] Q. Cao, H. P. Zhang, G. J. Wang, Q. Xia, Y. P. Wu, H. Q. Wu, *Electrochem. Commun.* **2007**, *9*, 1228.
[275] Y. Uno, K. Tachimori, T. Tsujikawa, T. Hirai, *ECS Trans.* **2010**, *25*, 121.
[276] H.-S. Kim, M. Kong, K. Kim, I.-J. Kim, H.-B. Gu, *J. Power Sources* **2007**, *171*, 917.
[277] Z.-Y. Chen, H.-L. Zhu, S. Ji, R. Fakir, V. Linkov, *Solid State Ionics* **2008**, *179*, 1810.
[278] S. Yang, P. Y. Zavalij, M. S Whittingham, *Electrochem. Commun.* **2001**, *3*, 505.
[279] R. Dominko, M. Bele, M. Gaberšček, M. Remskar, D. Hanzel, J. M. Goupil, S. Pejovnik, J. Jamnik, *J. Power Sources* **2006**, *153*, 274.
[280] C.-W. Ong, Y.-K. Lin, J.-S. Chen, *J. Electrochem. Soc.* **2007**, *154*, A527.
[281] Y. Wang, Y. Wang, E. Hosono, K. Wang, H. Zhou, *Angew. Chem., Int. Ed.* **2008**, *47*, 7461.
[282] J.-K. Kim, J.-W. Choi, G. S. Chauhan, J.-H. Ahn, G.-C. Hwang, J.-B. Choi, H.-J. Ahn, *Electrochim. Acta* **2008**, *53*, 8258.
[283] P. S. Herle, B. Ellis, N. Coombs, L. F. Nazar, *Nat. Mater.* **2004**, *3*, 147.
[284] T. Danner, M. Singh, S. Hein, J. Kaiser, H. Hahn, A. Latz, *J. Power Sources* **2016**, *334*, 191.
[285] M. Kroll, S. L. Karstens, M. Cronau, A. Hölzel, S. Schlabach, N. Nobel, C. Redenbach, B. Roling, U. Tallarek, *Batteries Supercaps* **2021**, *4*, 1363.

[286] R. Morasch, J. Landesfeind, B. Suthar, H. A. Gasteiger, *J. Electrochem. Soc.* **2018**, *165*, A3459.
[287] A. Chauhan, H. Nirschl, *Energy Technol.* **2023**, *11*, 2300281.
[288] M. J. Lain, J. Brandon, E. Kendrick, *Batteries* **2019**, *5*, 64.
[289] D. Witt, D. Wilde, F. Baakes, F. Belkhir, F. Röder, U. Krewer, *Energy Technol.* **2021**, *9*, 2000989.
[290] A. Kraytsberg, Y. Ein-Eli, *Adv. Energy Mater.* **2016**, *6*, 1600655.
[291] V. Wenzel, H. Nirschl, D. Nötzel, *Energy Technol.* **2015**, *3*, 692.
[292] Y. S. Zhang, N. E. Courtier, Z. Zhang, K. Liu, J. J. Bailey, A. M. Boyce, G. Richardson, P. R. Shearing, E. Kendrick, D. J. L. Brett, *Adv. Energy Mater.* **2022**, *12*, 2102233.
[293] J. Li, J. Fleetwood, W. B. Hawley, W. Kays, *Chem. Rev.* **2022**, *122*, 903.
[294] A. Väyrynen, J. Salminen, *J. Chem. Thermodyn.* **2012**, *46*, 80.
[295] W. B. Hawley, J. Li, *J. Energy Storage* **2019**, *25*, 100862.
[296] H. Liu, X. Cheng, Y. Chong, H. Yuan, J.-Q. Huang, Q. Zhang, *Particuology* **2021**, *57*, 56.
[297] R. Dominko, M. Gaberšček, J. Drofenik, M. Bele, J. Jamnik, *Electrochim. Acta* **2003**, *48*, 3709.
[298] R. Dominko, M. Gaberšček, J. Drofenik, M. Bele, S. Pejovnik, J. Jamnik, *J. Power Sources* **2003**, *119–121*, 770.
[299] D. Grießl, K. Huber, R. Scherbauer, A. Kwade, *Adv. Powder Technol.* **2021**, *32*, 2280.
[300] H. Zheng, G. Liu, X. Song, P. Ridgway, S. Xun, V. S. Battaglia, *J. Electrochem. Soc.* **2010**, *157*, A1060.
[301] E. Asylbekov, J. Mayer, H. Nirschl, A. Kwade, *Energy Technol.* **2023**, *11*, 2200867.
[302] A. Chauhan, E. Asylbekov, S. Kespe, H. Nirschl, *Electrochem. Sci. Adv.* **2023**, *3*, 100151.
[303] M. Chouchane, A. Rucci, T. Lombardo, A. C. Ngandjong, A. A. Franco, *J. Power Sources* **2019**, *444*, 227285.
[304] L. Zielke, T. Hutzenlaub, D. R. Wheeler, I. Manke, T. Arlt, N. Paust, R. Zengerle, S. Thiele, *Adv. Energy Mater.* **2014**, *4*, 1301617.
[305] H. Dreger, H. Bockholt, W. Haselrieder, A. Kwade, *J. Electron. Mater.* **2015**, *44*, 4434.
[306] B. Westphal, H. Bockholt, T. Günther, W. Haselrieder, A. Kwade, *ECS Trans.* **2015**, *64*, 57.
[307] H. Y. Tran, G. Greco, C. Täubert, M. Wohlfahrt-Mehrens, W. Haselrieder, A. Kwade, *J. Power Sources* **2012**, *210*, 276.
[308] N. Probst, E. Grivei, *Carbon* **2002**, *40*, 201.
[309] K. B. Singh, M. S. Tirumkudulu, *Phys. Rev. Lett.* **2007**, *98*, 218302.
[310] M. Singh, J. Kaiser, H. Hahn, *J. Electrochem. Soc.* **2015**, *162*, A1196.
[311] S. E. Cheon, C. W. Kwon, D. B. Kim, S. J. Hong, H. T. Kim, S. W. Kim, *Electrochim. Acta* **2000**, *46*, 599.
[312] I. Cho, J. Choi, K. Kim, M.-H. Ryou, Y. M. Lee, *RSC Adv.* **2015**, *5*, 95073.
[313] Y. Itou, N. Ogihara, S. Kawauchi, *J. Phys. Chem. C* **2020**, *124*, 5559.
[314] S. Luo, K. Wang, J. Wang, K. Jiang, Q. Li, S. Fan, *Adv. Mater.* **2012**, *24*, 2294.
[315] T.-S. Wei, B. Y. Ahn, J. Grotto, J. A. Lewis, *Adv. Mater.* **2018**, *30*, 1703027.
[316] K. Fu, Y. Wang, C. Yan, Y. Yao, Y. Chen, J. Dai, S. Lacey, Y. Wang, J. Wan, T. Li, Z. Wang, Y. Xu, L. Hu, *Adv. Mater.* **2016**, *28*, 2587.
[317] S. Y. Chew, S. H. Ng, J. Wang, P. Novák, F. Krumeich, S. L. Chou, J. Chen, H. K. Liu, *Carbon* **2009**, *47*, 2976.
[318] X. Li, F. Kang, W. Shen, *Carbon* **2006**, *44*, 1334.
[319] K. Sheem, Y. H. Lee, H. S. Lim, *J. Power Sources* **2006**, *158*, 1425.
[320] W. Guoping, Z. Qingtang, Y. Zuolong, Q. MeiZheng, *Solid State Ionics* **2008**, *179*, 263.
[321] A. Varzi, C. Täubert, M. Wohlfahrt-Mehrens, M. Kreis, W. Schütz, *J. Power Sources* **2011**, *196*, 3303.
[322] N. H. Kwon, D. Mouck-Makanda, K. M. Fromm, *Batteries* **2018**, *4*, 50.
[323] W. Wei, W. Lv, M.-B. Wu, F.-Y. Su, Y.-B. He, B. Li, F. Kang, Q.-H. Yang, *Carbon* **2013**, *57*, 530.
[324] X. Wang, Z. Feng, J. Huang, W. Deng, X. Li, H. Zhang, Z. Wen, *Carbon* **2018**, *127*, 149.
[325] K.-Y. Park, J.-M. Lim, N. S. Luu, J. R. Downing, S. G. Wallace, L. E. Chaney, H. Yoo, W. J. Hyun, H.-U. Kim, M. C. Hersam, *Adv. Energy Mater.* **2020**, *10*, 2001216.
[326] C. W. Park, J.-H. Lee, J. K. Seo, W. Y. Jo, D. Whang, S. M. Hwang, Y.-J. Kim, *Nat. Commun.* **2021**, *12*, 2145.
[327] J. Billaud, F. Bouville, T. Magrini, C. Villevieille, A. R. Studart, *Nat. Energy* **2016**, *1*, 16097.
[328] J. S. Sander, R. M. Erb, L. Li, A. Gurijala, Y. M. Chiang, *Nat. Energy* **2016**, *1*, 16099.
[329] R. Dubey, M.-D. Zwahlen, Y. Shynkarenko, S. Yakunin, A. Fuerst, M. V. Kovalenko, K. V. Kravchyk, *Batteries Supercaps* **2021**, *4*, 464.
[330] C.-J. Bae, C. K. Erdonmez, J. W. Halloran, Y.-M. Chiang, *Adv. Mater.* **2013**, *25*, 1254.
[331] J. D. Wilcox, M. M. Doeff, M. Marcinek, R. Kostecki, *J. Electrochem. Soc.* **2007**, *154*, A389.
[332] T. Mittermeier, A. Weiß, F. Hasché, H. A. Gasteiger, *J. Electrochem. Soc.* **2018**, *165*, F1349.
[333] R. Jung, M. Metzger, F. Maglia, C. Stinner, H. A. Gasteiger, *J. Electrochem. Soc.* **2017**, *164*, A1361.
[334] A. Guéguen, D. Streich, M. He, M. Mendez, F. F. Chesneau, P. Novák, E. J. Berg, *J. Electrochem. Soc.* **2016**, *163*, A1095.
[335] L. Wang, Y. Huang, R. Jiang, D. Jia, *J. Electrochem. Soc.* **2007**, *154*, A1015.
[336] A. Varzi, D. Bresser, J. von Zamory, F. Müller, S. Passerini, *Adv. Energy Mater.* **2014**, *4*, 1400054.
[337] J. F. Baumgärtner, M. Wörle, C. P. Guntlin, F. Krumeich, S. Siegrist, V. Vogt, D. C. Stoian, D. Chernyshov, W. van Beek, K. V. Kravchyk, M. V. Kovalenko, *Adv. Mater.* **2023**, *35*, 2304158.
[338] B. Wang, T. Liu, A. Liu, G. Liu, L. Wang, T. Gao, D. Wang, X. S. Zhao, *Adv. Energy Mater.* **2016**, *6*, 1600426.
[339] M. R. Palacín, *Chem. Soc. Rev.* **2009**, *38*, 2565.
[340] J. Wu, Y. Cao, H. Zhao, J. Mao, Z. Guo, *Carbon Energy* **2019**, *1*, 57.
[341] J. Lu, Z. Chen, F. Pan, Y. Cui, K. Amine, *Electrochem. Energy Rev.* **2018**, *1*, 35.
[342] K. Feng, M. Li, W. Liu, A. G. Kashkooli, X. Xiao, M. Cai, Z. Chen, *Small* **2018**, *14*, 1702737.
[343] Y. Zhao, L. P. Wang, M. T. Sougrati, Z. Feng, Y. Leconte, A. Fisher, M. Srinivasan, Z. Xu, *Adv. Energy Mater.* **2017**, *7*, 1601424.
[344] H.-J. Peng, Q. Zhang, *Angew. Chem., Int. Ed.* **2015**, *54*, 11018.
[345] F. Wu, G. Yushin, *Energy Environ. Sci.* **2017**, *10*, 435.
[346] A. R. Armstrong, P. G. Bruce, *Nature* **1996**, *381*, 499.
[347] S. Lee, Y. Cho, H.-K. Song, K. T. Lee, J. Cho, *Angew. Chem., Int. Ed.* **2012**, *51*, 8748.
[348] A. K. Padhi, K. S. Nanjundaswamy, J. B. Goodenough, *J. Electrochem. Soc.* **1997**, *144*, 1188.
[349] N.-H. Kwon, T. Drezen, I. Exnar, I. Teerlinck, M. Isono, M. Graetzel, *Electrochem. Solid-State Lett.* **2006**, *9*, A277.
[350] M. M. Ren, Z. Zhou, X. P. Gao, W. X. Peng, J. P. Wei, *J. Phys. Chem. C* **2008**, *112*, 5689.
[351] C. S. Yoon, M. H. Choi, B.-B. Lim, E.-J. Lee, Y.-K. Sun, *J. Electrochem. Soc.* **2015**, *162*, A2483.
[352] H.-J. Noh, S. Youn, C. S. Yoon, Y.-K. Sun, *J. Power Sources* **2013**, *233*, 121.
[353] M. Sathiya, K. Ramesha, G. Rousse, D. Foix, D. Gonbeau, A. S. Prakash, M. L. Doublet, K. Hemalatha, J. M. Tarascon, *Chem. Mater.* **2013**, *25*, 1121.
[354] Z. Lu, D. D. MacNeil, J. R. Dahn, *Electrochem. Solid-State Lett.* **2001**, *4*, A191.
[355] Z. Lu, L. Y. Beaulieu, R. A. Donaberger, C. L. Thomas, J. R. Dahn, *J. Electrochem. Soc.* **2002**, *149*, A778.

[356] J. Lee, A. Urban, X. Li, D. Su, G. Hautier, G. Ceder, *Science* **2014**, *343*, 519.
[357] R. J. Clément, Z. Lun, G. Ceder, *Energy Environ. Sci.* **2020**, *13*, 345.
[358] X.-F. Zhang, K.-X. Wang, X. Wei, J.-S. Chen, *Chem. Mater.* **2011**, *23*, 5290.
[359] J. S. Sakamoto, B. Dunn, *J. Electrochem. Soc.* **2002**, *149*, A26.
[360] C. Li, C. Yin, L. Gu, R. E. Dinnebier, X. Mu, P. A. van Aken, J. Maier, *J. Am. Chem. Soc.* **2013**, *135*, 11425.
[361] C. Li, L. Gu, J. Tong, S. Tsukimoto, J. Maier, *Adv. Funct. Mater.* **2011**, *21*, 1391.
[362] J. Cabana, L. Monconduit, D. Larcher, M. R. Palacín, *Adv. Mater.* **2010**, *22*, E170.
[363] H. Li, X. Huang, L. Chen, Z. Wu, Y. Liang, *Electrochem. Solid-State Lett.* **1999**, *2*, 547.
[364] Y.-S. Hu, R. Demir-Cakan, M.-M. Titirici, J.-O. Müller, R. Schlögl, M. Antonietti, J. Maier, *Angew. Chem., Int. Ed.* **2008**, *47*, 1645.
[365] L.-F. Cui, Y. Yang, C.-M. Hsu, Y. Cui, *Nano Lett.* **2009**, *9*, 3370.
[366] Y. Yao, M. T. McDowell, I. Ryu, H. Wu, N. Liu, L. Hu, W. D. Nix, Y. Cui, *Nano Lett.* **2011**, *11*, 2949.
[367] N. Liu, H. Wu, M. T. McDowell, Y. Yao, C. Wang, Y. Cui, *Nano Lett.* **2012**, *12*, 3315.
[368] Y. Idota, T. Kubota, A. Matsufuji, Y. Maekawa, T. Miyasaka, *Science* **1997**, *276*, 1395.
[369] X. W. Lou, Y. Wang, C. Yuan, J. Y. Lee, L. A. Archer, *Adv. Mater.* **2006**, *18*, 2325.
[370] X. Zhou, L.-J. Wan, Y.-G. Guo, *Adv. Mater.* **2013**, *25*, 2152.
[371] W.-M. Zhang, J.-S. Hu, Y.-G. Guo, S.-F. Zheng, L.-S. Zhong, W.-G. Song, L.-J. Wan, *Adv. Mater.* **2008**, *20*, 1160.
[372] J. Yang, M. Winter, J. O. Besenhard, *Solid State Ionics* **1996**, *90*, 281.
[373] K. Kravchyk, L. Protesescu, M. I. Bodnarchuk, F. Krumeich, M. Yarema, M. Walter, C. Guntlin, M. V. Kovalenko, *J. Am. Chem. Soc.* **2013**, *135*, 4199.
[374] M. He, K. Kravchyk, M. Walter, M. V. Kovalenko, *Nano Lett.* **2014**, *14*, 1255.
[375] G. Zheng, S. W. Lee, Z. Liang, H.-W. Lee, K. Yan, H. Yao, H. Wang, W. Li, S. Chu, Y. Cui, *Nat. Nanotechnol.* **2014**, *9*, 618.
[376] K. Yan, Z. Lu, H.-W. Lee, F. Xiong, P.-C. Hsu, Y. Li, J. Zhao, S. Chu, Y. Cui, *Nat. Energy* **2016**, *1*, 16010.
[377] M. N. Obrovac, L. J. Krause, *J. Electrochem. Soc.* **2007**, *154*, A103.
[378] L. Y. Beaulieu, K. W. Eberman, R. L. Turner, L. J. Krause, J. R. Dahn, *Electrochem. Solid-State Lett.* **2001**, *4*, A137.
[379] X. H. Liu, L. Zhong, S. Huang, S. X. Mao, T. Zhu, J. Y. Huang, *ACS Nano* **2012**, *6*, 1522.
[380] X. Ji, K. T. Lee, L. F. Nazar, *Nat. Mater.* **2009**, *8*, 500.
[381] H. Wang, Y. Yang, Y. Liang, J. T. Robinson, Y. Li, A. Jackson, Y. Cui, H. Dai, *Nano Lett.* **2011**, *11*, 2644.
[382] N. Jayaprakash, J. Shen, S. S. Moganty, A. Corona, L. A. Archer, *Angew. Chem., Int. Ed.* **2011**, *50*, 5904.
[383] C. Liang, N. J. Dudney, J. Y. Howe, *Chem. Mater.* **2009**, *21*, 4724.
[384] B. Zhang, X. Qin, G. R. Li, X. P. Gao, *Energy Environ. Sci.* **2010**, *3*, 1531.
[385] R. Elazari, G. Salitra, A. Garsuch, A. Panchenko, D. Aurbach, *Adv. Mater.* **2011**, *23*, 5641.
[386] N. Yamakawa, M. Jiang, B. Key, C. P. Grey, *J. Am. Chem. Soc.* **2009**, *131*, 10525.
[387] C. Li, L. Gu, S. Tsukimoto, P. A. van Aken, J. Maier, *Adv. Mater.* **2010**, *22*, 3650.
[388] S.-W. Kim, D.-H. Seo, H. Gwon, J. Kim, K. Kang, *Adv. Mater.* **2010**, *22*, 5260.
[389] F. Wang, R. Robert, N. A. Chernova, N. Pereira, F. Omenya, F. Badway, X. Hua, M. Ruotolo, R. Zhang, L. Wu, V. Volkov, D. Su, B. Key, M. S. Whittingham, C. P. Grey, G. G. Amatucci, Y. Zhu, J. Graetz, *J. Am. Chem. Soc.* **2011**, *133*, 18828.
[390] F. Wu, V. Srot, S. Chen, S. Lorger, P. A. van Aken, J. Maier, Y. Yu, *Adv. Mater.* **2019**, *31*, 1905146.
[391] C. P. Guntlin, T. Zünd, K. V. Kravchyk, M. Wörle, M. I. Bodnarchuk, M. V. Kovalenko, *J. Mater. Chem. A* **2017**, *5*, 7383.
[392] K. V. Kravchyk, T. Zünd, M. Wörle, M. V. Kovalenko, M. I. Bodnarchuk, *Chem. Mater.* **2018**, *30*, 1825.
[393] X. Zhao, C. M. Hayner, M. C. Kung, H. H. Kung, *Chem. Commun.* **2012**, *48*, 9909.
[394] L. Li, F. Meng, S. Jin, *Nano Lett.* **2012**, *12*, 6030.
[395] R. Ma, M. Wang, P. Tao, Y. Wang, C. Cao, G. Shan, S. Yang, L. Xi, J. C. Y. Chung, Z. Lu, *J. Mater. Chem. A* **2013**, *1*, 15060.
[396] R. Ma, Z. Lu, C. Wang, H.-E. Wang, S. Yang, L. Xi, J. C. Y. Chung, *Nanoscale* **2013**, *5*, 6338.
[397] B. Li, D. W. Rooney, N. Zhang, K. Sun, *ACS Appl. Mater. Interfaces* **2013**, *5*, 5057.
[398] W. Fu, E. Zhao, Z. Sun, X. Ren, A. Magasinski, G. Yushin, *Adv. Funct. Mater.* **2018**, *28*, 1801711.
[399] X. Wang, W. Gu, J. T. Lee, N. Nitta, J. Benson, A. Magasinski, M. W. Schauer, G. Yushin, *Small* **2015**, *11*, 5164.
[400] K. Rui, Z. Wen, Y. Lu, J. Jin, C. Shen, *Adv. Energy Mater.* **2015**, *5*, 1401716.
[401] F. Badway, A. N. Mansour, N. Pereira, J. F. Al-Sharab, F. Cosandey, I. Plitz, G. G. Amatucci, *Chem. Mater.* **2007**, *19*, 4129.
[402] J. F. Baumgärtner, F. Krumeich, M. Wörle, K. V. Kravchyk, M. V. Kovalenko, *Commun. Chem.* **2022**, *5*, 6.
[403] A. J. Gmitter, F. Badway, S. Rangan, R. A. Bartynski, A. Halajko, N. Pereira, G. G. Amatucci, *J. Mater. Chem.* **2010**, *20*, 4149.
[404] M. Bervas, A. N. Mansour, W. S. Yoon, J. F. Al-Sharab, F. Badway, F. Cosandey, L. C. Klein, G. G. Amatucci, *J. Electrochem. Soc.* **2006**, *153*, A799.
[405] M. Bervas, F. Badway, L. C. Klein, G. G. Amatucci, *Electrochem. Solid-State Lett.* **2005**, *8*, A179.
[406] M. F. Oszajca, K. V. Kravchyk, M. Walter, F. Krieg, M. I. Bodnarchuk, M. V. Kovalenko, *Nanoscale* **2015**, *7*, 16601.
[407] P. Poizot, S. Laruelle, S. Grugeon, L. Dupont, J. M. Tarascon, *Nature* **2000**, *407*, 496.
[408] Y. Li, B. Tan, Y. Wu, *Nano Lett.* **2008**, *8*, 265.
[409] Z.-S. Wu, W. Ren, L. Wen, L. Gao, J. Zhao, Z. Chen, G. Zhou, F. Li, H.-M. Cheng, *ACS Nano* **2010**, *4*, 3187.
[410] S. Yang, X. Feng, S. Ivanovici, K. Müllen, *Angew. Chem., Int. Ed.* **2010**, *49*, 8408.
[411] W.-M. Zhang, X.-L. Wu, J.-S. Hu, Y.-G. Guo, L.-J. Wan, *Adv. Funct. Mater.* **2008**, *18*, 3941.
[412] G. Zhou, D.-W. Wang, F. Li, L. Zhang, N. Li, Z.-S. Wu, L. Wen, G. Q. Lu, H.-M. Cheng, *Chem. Mater.* **2010**, *22*, 5306.
[413] X. Zhu, Y. Zhu, S. Murali, M. D. Stoller, R. S. Ruoff, *ACS Nano* **2011**, *5*, 3333.
[414] Z. Wang, D. Luan, S. Madhavi, Y. Hu, X. W. Lou, *Energy Environ. Sci.* **2012**, *5*, 5252.
[415] C. He, S. Wu, N. Zhao, C. Shi, E. Liu, J. Li, *ACS Nano* **2013**, *7*, 4459.
[416] C. Lei, F. Han, D. Li, W.-C. Li, Q. Sun, X.-Q. Zhang, A.-H. Lu, *Nanoscale* **2013**, *5*, 1168.
[417] A. L. M. Reddy, M. M. Shaijumon, S. R. Gowda, P. M. Ajayan, *Nano Lett.* **2009**, *9*, 1002.
[418] H. Wang, L.-F. Cui, Y. Yang, H. Sanchez Casalongue, J. T. Robinson, Y. Liang, Y. Cui, H. Dai, *J. Am. Chem. Soc.* **2010**, *132*, 13978.
[419] X.-Y. Shan, G. Zhou, L.-C. Yin, W.-J. Yu, F. Li, H.-M. Cheng, *J. Mater. Chem. A* **2014**, *2*, 17808.
[420] D. Wang, D. Choi, J. Li, Z. Yang, Z. Nie, R. Kou, D. Hu, C. Wang, L. V. Saraf, J. Zhang, I. A. Aksay, J. Liu, *ACS Nano* **2009**, *3*, 907.
[421] R. Fang, G. Li, S. Zhao, L. Yin, K. Du, P. Hou, S. Wang, H.-M. Cheng, C. Liu, F. Li, *Nano Energy* **2017**, *42*, 205.

[422] P. R. Kumar, M. Venkateswarlu, M. Misra, A. K. Mohanty, N. Satyanarayana, *Ionics* **2013**, *19*, 461.
[423] F. Wang, J. Yang, P. Gao, Y. NuLi, J. Wang, *J. Power Sources* **2011**, *196*, 10258.
[424] J. Ni, Y. Kawabe, M. Morishita, M. Watada, T. Sakai, *J. Power Sources* **2011**, *196*, 8104.
[425] Y. Jiang, R. Liu, W. Xu, Z. Jiao, M. Wu, Y. Chu, L. Su, H. Cao, M. Hou, B. Zhao, *J. Mater. Res.* **2013**, *28*, 2584.
[426] X.-M. Liu, Z.-D. Huang, S. Oh, P.-C. Ma, P. C. H. Chan, G. K. Vedam, K. Kang, J.-K. Kim, *J. Power Sources* **2010**, *195*, 4290.
[427] Z. Lu, N. Liu, H.-W. Lee, J. Zhao, W. Li, Y. Li, Y. Cui, *ACS Nano* **2015**, *9*, 2540.
[428] Z. Sun, S. Fang, Y. H. Hu, *Chem. Rev.* **2020**, *120*, 10336.
[429] H. Sun, J. Zhu, D. Baumann, L. Peng, Y. Xu, I. Shakir, Y. Huang, X. Duan, *Nat. Rev. Mater.* **2019**, *4*, 45.
[430] T. Liu, L. Zhang, B. Cheng, J. Yu, *Adv. Energy Mater.* **2019**, *9*, 1803900.
[431] A. Fu, C. Wang, F. Pei, J. Cui, X. Fang, N. Zheng, *Small* **2019**, *15*, 1804786.
[432] J. Mao, J. Iocozzia, J. Huang, K. Meng, Y. Lai, Z. Lin, *Energy Environ. Sci.* **2018**, *11*, 772.
[433] X. Yao, Y. Zhao, *Chem* **2017**, *2*, 171.
[434] X. H. Xia, D. L. Chao, Y. Q. Zhang, Z. X. Shen, H. J. Fan, *Nano Today* **2014**, *9*, 785.
[435] L. Jiang, Z. Fan, *Nanoscale* **2014**, *6*, 1922.
[436] S. Han, D. Wu, S. Li, F. Zhang, X. Feng, *Adv. Mater.* **2014**, *26*, 849.
[437] F. Zhang, T. Zhang, X. Yang, L. Zhang, K. Leng, Y. Huang, Y. Chen, *Energy Environ. Sci.* **2013**, *6*, 1623.
[438] J. Luo, J. Liu, Z. Zeng, C. F. Ng, L. Ma, H. Zhang, J. Lin, Z. Shen, H. J. Fan, *Nano Lett.* **2013**, *13*, 6136.
[439] X. Cao, Y. Shi, W. Shi, X. Rui, Q. Yan, J. Kong, H. Zhang, *Small* **2013**, *9*, 3433.
[440] Z. Deng, H. Jiang, Y. Hu, Y. Liu, L. Zhang, H. Liu, C. Li, *Adv. Mater.* **2017**, *29*, 1603020.
[441] S. Kim, J. Liu, K. Sun, J. Wang, S. J. Dillon, P. V. Braun, *Adv. Funct. Mater.* **2017**, *27*, 1702783.
[442] Z. Chen, W. Ren, L. Gao, B. Liu, S. Pei, H.-M. Cheng, *Nat. Mater.* **2011**, *10*, 424.
[443] B. Li, S. Li, J. Xu, S. Yang, *Energy Environ. Sci.* **2016**, *9*, 2025.
[444] J. Wang, J. Liu, D. Chao, J. Yan, J. Lin, Z. X. Shen, *Adv. Mater.* **2014**, *26*, 7162.
[445] M. Chen, J. Liu, D. Chao, J. Wang, J. Yin, J. Lin, H. J Fan, Z. Xiang Shen, *Nano Energy* **2014**, *9*, 364.
[446] F. Zhou, S. Xin, H.-W. Liang, L.-T. Song, S.-H. Yu, *Angew. Chem., Int. Ed.* **2014**, *53*, 11552.
[447] X. Fan, Y. Zhu, C. Luo, L. Suo, Y. Lin, T. Gao, K. Xu, C. Wang, *ACS Nano* **2016**, *10*, 5567.
[448] J. Liang, X.-Y. Yu, H. Zhou, H. B. Wu, S. Ding, X. W. Lou, *Angew. Chem., Int. Ed.* **2014**, *53*, 12803.
[449] M. Yan, F. Wang, C. Han, X. Ma, X. Xu, Q. An, L. Xu, C. Niu, Y. Zhao, X. Tian, P. Hu, H. Wu, L. Mai, *J. Am. Chem. Soc.* **2013**, *135*, 18176.
[450] H. Wu, G. Zheng, N. Liu, T. J. Carney, Y. Yang, Y. Cui, *Nano Lett.* **2012**, *12*, 904.
[451] G. Zheng, Y. Yang, J. J. Cha, S. S. Hong, Y. Cui, *Nano Lett.* **2011**, *11*, 4462.
[452] Y. Yu, L. Gu, C. Wang, A. Dhanabalan, P. A. van Aken, J. Maier, *Angew. Chem., Int. Ed.* **2009**, *48*, 6485.
[453] Z.-S. Wu, D.-W. Wang, W. Ren, J. Zhao, G. Zhou, F. Li, H.-M. Cheng, *Adv. Funct. Mater.* **2010**, *20*, 3595.
[454] Q. Chu, Z. Xing, X. Ren, A. M. Asiri, A. O. Al-Youbi, K. A. Alamry, X. Sun, *Electrochim. Acta* **2013**, *111*, 80.
[455] Y. Shen, X. Wang, H. Hu, M. Jiang, X. Yang, H. Shu, *J. Power Sources* **2015**, *283*, 204.
[456] K. Zhao, L. Zhang, R. Xia, Y. Dong, W. Xu, C. Niu, L. He, M. Yan, L. Qu, L. Mai, *Small* **2016**, *12*, 588.
[457] Z. Wang, Y. Dong, H. Li, Z. Zhao, H. Bin Wu, C. Hao, S. Liu, J. Qiu, X. W. Lou, *Nat. Commun.* **2014**, *5*, 5002.
[458] L. Zhang, D. Liu, Z. Muhammad, F. Wan, W. Xie, Y. Wang, L. Song, Z. Niu, J. Chen, *Adv. Mater.* **2019**, *31*, 1903955.
[459] Z. Du, X. Chen, W. Hu, C. Chuang, S. Xie, A. Hu, W. Yan, X. Kong, X. Wu, H. Ji, L.-J. Wan, *J. Am. Chem. Soc.* **2019**, *141*, 3977.
[460] A. L. M. Reddy, A. Srivastava, S. R. Gowda, H. Gullapalli, M. Dubey, P. M. Ajayan, *ACS Nano* **2010**, *4*, 6337.
[461] Z.-S. Wu, W. Ren, L. Xu, F. Li, H.-M. Cheng, *ACS Nano* **2011**, *5*, 5463.
[462] L. Qie, W.-M. Chen, Z.-H. Wang, Q.-G. Shao, X. Li, L.-X. Yuan, X.-L. Hu, W.-X. Zhang, Y.-H. Huang, *Adv. Mater.* **2012**, *24*, 2047.
[463] E. Frackowiak, F. Béguin, *Carbon* **2002**, *40*, 1775.
[464] E. Yoo, J. Kim, E. Hosono, H.-S. Zhou, T. Kudo, I. Honma, *Nano Lett.* **2008**, *8*, 2277.
[465] G. Wang, X. Shen, J. Yao, J. Park, *Carbon* **2009**, *47*, 2049.

Julian F. Baumgärtner received his Bachelor in chemistry from Albert-Ludwigs University Freiburg (Germany) in 2019 and his Master's in chemistry from ETH Zurich in 2021. He carried out projects in the groups of Prof. Christophe Copéret and Prof. Christoph Müller before completing his Master Thesis under the supervision of Prof. Maksym Kovalenko. Julian joined the group for his Ph.D. studies the following year, focusing on novel conversion-type cathode materials for Li-ion and post-Li-ion batteries.

Kostiantyn V. Kravchyk obtained his Ph.D. degree from Vernadsky Institute of General and Inorganic Chemistry of the Ukrainian National Academy of Sciences in 2009. Then, he completed postdoctoral research at the University of Le Mans (France), the University of Nantes (France), and ETH Zurich and Empa (Swiss Federal Laboratories for Materials Science and Technology). He now works as a senior scientist at ETH Zurich and Empa in the Functional Inorganic Materials group of Prof. Maksym Kovalenko. His research interests include all-solid-state Li-ion batteries, novel concepts for electrochemical energy storage, and novel materials for Li-ion and post-Li-ion batteries.

Maksym V. Kovalenko, born in 1982, studied chemistry at Chernivtsi National University (Ukraine) and then continued his studies at the Johannes Kepler University Linz (Austria), earning his Ph.D. degree in 2007 with professor Dr. Wolfgang Heiss. Subsequently, he joined the University of Chicago for postdoctoral training with Prof. Dmitri Talapin (research topic: inorganic ligand capping of colloidal nanocrystals). He joined ETH Zurich in summer 2011 as an assistant professor at the Laboratory of Inorganic Chemistry. Since August 2020, he has been a full professor. His group is also affiliated with Empa (Swiss Federal Laboratories for Materials Science and Technology). The research activities of Maksym Kovalenko and his group focus on chemistry, physics, and applications of inorganic solid-state materials and nanostructures.